Published December 29, 2014

Mechanism of activation of the prokaryotic channel ELIC by propylamine: A single-channel study

Alessandro Marabelli, Remigijus Lape, and Lucia Sivilotti

Department of Neuroscience, Physiology and Pharmacology, University College London, London WC1E 6BT, England, UK

Prokaryotic channels, such as *Erwinia chrysanthemi* ligand-gated ion channel (ELIC) and *Gloeobacter violaceus* ligand-gated ion channel, give key structural information for the pentameric ligand-gated ion channel family, which includes nicotinic acetylcholine receptors. ELIC, a cationic channel from *E. chrysanthemi*, is particularly suitable for single-channel recording because of its high conductance. Here, we report on the kinetic properties of ELIC channels expressed in human embryonic kidney 293 cells. Single-channel currents elicited by the full agonist propylamine (0.5–50 mM) in outside-out patches at −60 mV were analyzed by direct maximum likelihood fitting of kinetic schemes to the idealized data. Several mechanisms were tested, and their adequacy was judged by comparing the predictions of the best fit obtained with the observable features of the experimental data. These included open-/shut-time distributions and the time course of macroscopic propylamine-activated currents elicited by fast theta-tube applications (50–600 ms, 1–50 mM, −100 mV). Related eukaryotic channels, such as glycine and nicotinic receptors, when fully liganded open with high efficacy to a single open state, reached via a preopening intermediate. The simplest adequate description of their activation, the "Flip" model, assumes a concerted transition to a single intermediate state at high agonist concentration. In contrast, ELIC open-time distributions at saturating propylamine showed multiple components. Thus, more than one open state must be accessible to the fully liganded channel. The "Primed" model allows opening from multiple fully liganded intermediates. The best fits of this type of model showed that ELIC maximum open probability (99%) is reached when at least two and probably three molecules of agonist have bound to the channel. The overall efficacy with which the fully liganded channel opens was ∼102 (∼20 for α1β glycine channels). The microscopic affinity for the agonist increased as the channel activated, from 7 mM for the resting state to 0.15 mM for the partially activated intermediate state.

INTRODUCTION

The ultimate aim of channel kinetics is to identify and measure each step in the activation of a channel and map these steps to specific changes in the structure of the protein. Progress toward this goal requires combining the information that comes from detailed mechanistic modeling (from functional data such as single-channel recordings and fast agonist or voltage relaxations) together with information about the channel structure and the conformational states it can access.

In the Cys-loop family of pentameric ligand-gated ion channels (pLGICs), decades of recording single-channel data and of refining analysis techniques have produced detailed reaction schemes that describe the activation of several of the major synaptic channels. For muscle nicotinic receptors and glycine receptors, we know that two or three molecules of transmitter, respectively, must bind to open the channel with maximum efficacy, and in those circumstances the open probability (P_{open}) is very high, >95%. Synaptic channels open very quickly when the neurotransmitter binds, but refinement in model-fitting techniques has allowed us to detect one or more intermediate states between agonist binding and channel opening. In these states the channel is still closed, but its affinity for the agonist has already increased from its resting value (Burzomato et al., 2004; Mukhtasimova et al., 2009; Jadey and Auerbach, 2012). The systematic analysis of muscle nicotinic receptor mutants suggests that the perturbation introduced by agonist binding may spread in several discrete steps from the extracellular domain to the channel gate (Grosman et al., 2000; Purohit et al., 2007).

Making structural sense of these findings is not straightforward, and we still do not know the exact nature and sequence of the channel conformational changes upon activation, or the structural correlates of the intermediate states detected by single-channel analysis, despite the first solution of both shut and open structures for the same channel, recently obtained for *Gloeobacter violaceus* ligand-gated ion channel (GLIC; Sauguet et al., 2014).

Correspondence to Lucia Sivilotti: l.sivilotti@ucl.ac.uk

Abbreviations used in this paper: ELIC, *Erwinia chrysanthemi* ligand-gated ion channel; GLIC, *Gloeobacter violaceus* ligand-gated ion channel; HEK, human embryonic kidney; J&W, Jones and Westbrook; MWC, Monod–Wyman–Changeux; n_H, Hill coefficient; pLGIC, pentameric ligand-gated ion channel; P_{open}, open probability; t_{crit}, critical shut time.

The Rockefeller University Press $30.00
J. Gen. Physiol. Vol. 145 No. 1 23–45
www.jgp.org/cgi/doi/10.1085/jgp.201411234

Supplemental Material can be found at:
http://jgp.rupress.org/content/suppl/2014/12/24/jgp.201411234.DC1.html

Published December 29, 2014

One of the problems is that some of the best structural data come from channels for which we have no single-channel kinetics, such as the prokaryotic channels GLIC and *Erwinia chrysanthemi* ligand-gated ion channel (ELIC; Hilf and Dutzler, 2008, 2009b; Bocquet et al., 2009) and the nematode channel GluCl (Hibbs and Gouaux, 2011). Obtaining a detailed understanding of the activation mechanism of one of these channels might help with the task of mapping structure to function. This paper is the first single-channel kinetic characterization of ELIC.

MATERIALS AND METHODS

Cell culture and transfection of cells

Human embryonic kidney (HEK)293 cells, obtained from the ATCC, were maintained in a humidified incubator at 37°C (95% air/5% CO_2) in Dulbecco's modified Eagle's medium supplemented with: sodium pyruvate (0.11 g/liter), heat-inactivated fetal bovine serum (10% vol/vol), and 100 U/ml penicillin G/100 µg/ml streptomycin sulfate (all from Invitrogen). Cells were plated onto polylysine-coated glass coverslips, in 35-mm culture dishes containing 2 ml Dulbecco's modified Eagle's medium. HEK293 cells were transfected by a Ca^{2+}-phosphate coprecipitation method (Groot-Kormelink et al., 2002) with two pcDNA3 plasmids (Invitrogen), one encoding the ELIC protein (UniProt accession no. P0C7B7) and the other coding for the enhanced green fluorescent protein (eGFP; Takara Bio Inc.). The mixture of cDNA used for the cell transfection contained 5–82% ELIC receptor cDNA and 18% eGFP cDNA. The remainder was empty vector (i.e., without the coding insert), in appropriate proportion to obtain the desired expression level. The total amount of the final cDNA mixture was 3 µg per plate. Recordings were performed between 4 h and 2 d after washing off the transfection medium. The ELIC construct was provided by R. Dutzler and I. Zimmermann (University of Zürich, Zürich, Switzerland; Zimmermann and Dutzler, 2011).

Electrophysiological recordings

All electrophysiological recordings were obtained using patch-clamp recording in two different configurations: (1) whole cell for macroscopic current dose–response curves and (2) outside-out for macroscopic currents elicited by fast agonist application and for single-channel recordings. Patch-clamp pipettes were pulled from thick-walled borosilicate capillaries (with filament; Harvard Apparatus), and tips were fire polished to obtain a final pipette resistance of 3–5 MΩ (whole cell) or 8–12 MΩ (outside-out). In addition, pipettes for single-channel recording were coated near the tip with Sylgard (Corning). For whole-cell recordings, the access resistance was never >8 MΩ and was compensated by at least 75%.

The bath solution (for all recording configurations) was composed as follows (mM): 150 KCl, 0.5 $BaCl_2$, and 10 HEPES, with pH adjusted to 7.4 with KOH and osmolarity of 300 mOsm. The pipette solution was identical to the extracellular solution. Junction potential was calculated to be around 0 mV (Clampex 10.2; Molecular Devices). In our solutions we had barium (at a low concentration of 0.5 mM) rather than calcium, because barium is less potent than calcium in inhibiting ELIC activation (Zimmermann et al., 2012). This allowed us to characterize the full range of channel activity without exceeding 100-mM agonist concentrations. All solutions were prepared from bi-distilled water and filtered through a 0.2-µm Cyclopore track-etched membrane (GE Healthcare) to remove impurities. All electrophysiological recordings were done at a temperature of 19–21°C.

Currents were recorded with an Axopatch 200B amplifier (Molecular Devices). Recordings were prefiltered at 5 kHz (for macroscopic currents) or 10 KHz (single-channel currents) with a four-pole low-pass Bessel filter (built in the amplifier), digitized with Digidata 1322A (sampling rate of 20 kHz for macroscopic currents and 100 kHz for single-channel currents; Molecular Devices), and stored directly on the computer hard drive via Clampex 10.2 software (Molecular Devices).

Concentration–response curves

Whole-cell currents elicited by local U-tube application (Krishtal and Pidoplichko, 1980) of 0.1–5 mM propylamine were recorded at a holding potential of −30 mV. The U-tube position was optimized before the experiment by the application of diluted bath solution (e.g., 30:70 bath solution/water) to an open-tipped recording pipette. The exchange time was normally between 50 and 100 ms. A full concentration–response curve was obtained in each cell. To monitor the rundown/run-up of responses during recording, a standard concentration of propylamine (0.5 mM) was applied every third response. Only cells in which the rundown was <20% were accepted for further analysis, and no correction for rundown was applied. The Hill equation was fitted to each individual concentration–response curve (program CVFIT) to estimate EC_{50} and Hill coefficient (n_H) values. For the purpose of display only, responses were then normalized to the fitted maximum in each cell. These normalized responses were pooled and refitted with the Hill equation for the display in Fig. 1.

Fast agonist application

Macroscopic currents, evoked in outside-out patches by fast agonist application pulses, were recorded at a nominal pipette holding potential of −100 mV. Propylamine, dissolved in the bath solution, was applied to outside-out patches with a theta tube (Hilgenberg GmbH) cut to a final diameter of ∼150 µm at the tip. The tube was driven by a piezo stepper (Burleigh Instruments, Inc.). The exchange time was measured by the application of diluted bath solution (e.g., 30:70 bath solution/water) before the experiment (to optimize the electrode position) and after the rupture of the patch. During all macroscopic recording experiments, the bath was also perfused at a rate of 1 or 5 ml per minute (for fast outside-out agonist applications or whole-cell recordings, respectively).

To study the kinetics of macroscopic currents, 10–20 responses were recorded in response to pulses of propylamine applied at intervals of at least 10 s. For each patch, responses were averaged, excluding failures or responses that contained patch breakdowns. Only experiments in which the rundown between the first and last three responses was <30% were included in the analysis. The rise and decay times for open-tip currents were measured as the time from 20 to 80% of the peak response using Clampfit 10.2 software (Molecular Devices). Patches in which the open-tip response had a 20–80% exchange time slower than 250 µs were rejected from further analysis. The time course of activation/deactivation of the macroscopic currents between 20 and 80% (or 80 to 20%) of peak response was fitted with one or the sum of several exponentials.

Using the rate constant values from the fit of each set of single-channel data with the different models, we calculated macroscopic currents as responses to concentration pulses using the DC-PyPs program. Realistic profile concentration pulses had rising and falling phases of 200 µs (20–80% rise/fall time) described by an error function. Responses to 1, 10, and 50 mM propylamine were calculated for the fitted mechanisms and the sets of rate constant values obtained from the three independent datasets fitted. Averages of currents calculated from the three sets are displayed in Fig. 9 (B and D). The relation between agonist concentration and current rise time constant was calculated for the fits to each dataset and averaged for the display in Fig. 9 E. The time constant of

Published December 29, 2014

decay of the calculated currents was measured in the same way as for the experimental ones and is displayed in Fig. 9 F.

Single-channel currents

All single-channel recordings were performed in outside-out configuration. The agonist (0.3–100 mM propylamine) was applied via dish perfusion. The bath level was kept as low as possible to reduce noise. Currents were recorded at a pipette potential of −60 mV. For offline analysis, data were filtered digitally (low-pass Gaussian filter) using the program Clampfit 10.2 to achieve a final cutoff frequency of 3–6 kHz.

Recordings were idealized (6,000–24,000 transitions per patch) by time-course fitting with the program SCAN. Segments showing seal breakdowns or dubious channel openings were excluded, and those intervals were marked unusable. Afterward, we imposed a temporal resolution between 25 and 40 µs depending on the signal-to-noise level obtained during the recording. The temporal resolution is the duration of the shortest event that can be reliably detected, and its value is taken into account in implementing the exact solution for missed events correction by Hawkes et al. (1990, 1992). Given that we observed a marked rundown in outside-out macroscopic currents, we checked particularly carefully the stability of the single-channel activity over time and found that average open/shut times remained stable for up to 20–30 min. Patches were analyzed further only if the amplitudes of channel openings and the open and shut times were stable through the recording. Observed open/shut times are periods during which the channel appears to be continuously open/shut (at the experimental resolution). The presence of shuttings and openings too short to be unambiguously resolved lengthens observed open and shut times versus their true duration.

After imposing the resolution, all the open/shut times collected in the idealization were plotted as histograms and empirically fitted by exponential probability density functions (EKDIST program). This allowed us to check that distributions were consistent across patches at the same agonist concentration and to proceed to the next stage of the analysis and determine a suitable value for the critical shut time (t_{crit}). This value is chosen to divide recordings into segments that are likely to arise from the activity of only one channel molecule.

To evaluate kinetic schemes and obtain the rate constants associated with them, maximum likelihood fitting was performed with the HJCFIT program (Colquhoun et al., 1996, 2003). Idealized single-channel records were grouped into three sets. Each set consisted of four patches at different propylamine concentrations (0.5, 1, 5, and 10 mM), and the data from the four patches in each set were fitted simultaneously. Openings in each idealized record were divided into groups using a t_{crit} value for shut times, and only shut times shorter than t_{crit} were used for fitting. The longer shut times cannot provide information about the rate constants in the mechanism because they are distorted by the number of channels in the patch. For lower concentrations of agonist (0.5–5 mM), where groups of openings can be treated as "bursts"—groups of openings terminated by agonist unbinding—some of that information was recovered by using in the likelihood calculation Colquhoun Hawkes and Szrodzinski vectors, a particular form of initial and final occupancy matrices (Colquhoun et al., 1996). This adjustment to the calculations exploits the fact that having more than one channel in the patch can only shorten the apparent shut time. Thus, the "real" shut time, which would be between two openings of the same channel molecule, has got to be at least as long as the observed shut time (Colquhoun et al., 1996), and

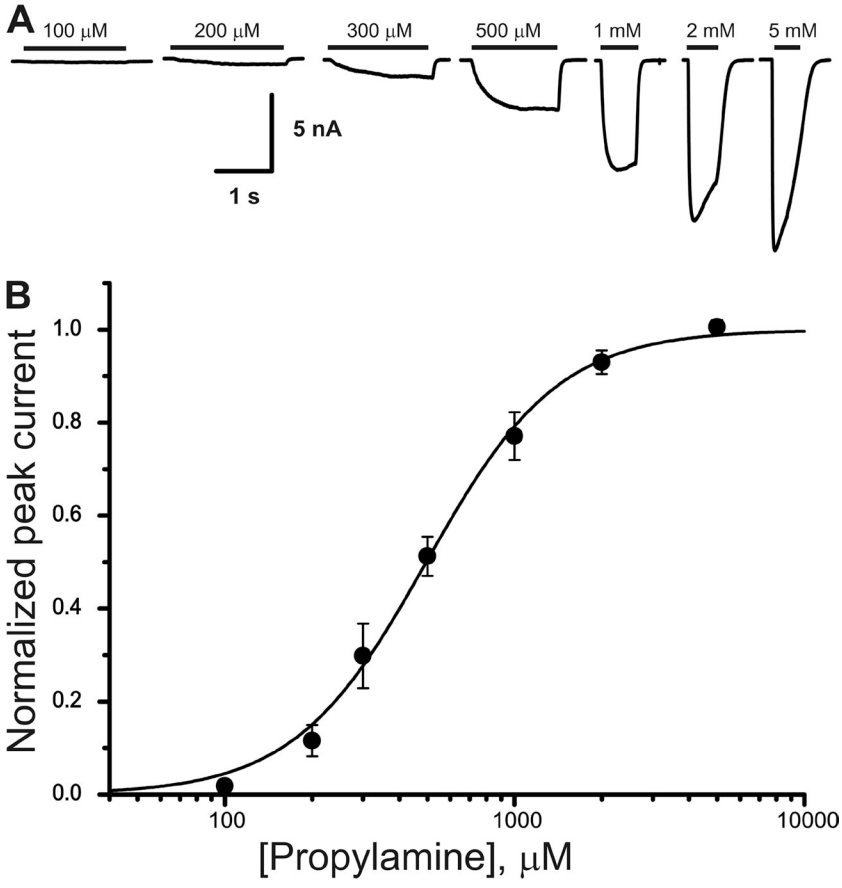

Figure 1. The whole-cell concentration–response curve for the ELIC agonist propylamine. (A) Representative macroscopic currents elicited by U-tube application (horizontal bars above the traces) of propylamine to ELIC-expressing HEK293 cells held at −30 mV. (B) Average concentration–response curve for propylamine (n = 4 cells). Individual dose–response curves were obtained in each cell, and responses were measured at their peak and normalized to the fitted maximum. Normalized curves were then averaged and fitted with the Hill equation (EC_{50} = 500 ± 100 µM; n_H = 2.2 ± 0.1; maximum current = 9 ± 2 nA). Error bars depict the standard deviation of the mean.

Published December 29, 2014

this information provides a boundary condition that has been demonstrated to improve the effectiveness of estimation (see Colquhoun et al., 2003). At high concentrations (>5 mM), t_{crit} divides record in "clusters" of openings, groups of openings separated by sojourns in long-lived desensitization states (as defined in Sakmann et al., 1980).

The maximum likelihood fits were performed using the HJCFIT program. This optimizes a likelihood function for a dataset (with four concentrations) of idealized sequences of events in chronological order of occurrence, given the postulated model and the initial guesses for the rate constant values, and taking into account the imposed resolution. Fits were repeated using several different sets of initial guesses to check the consistency of the maximum value of the likelihood. To test the quality of the fits, we calculated open-time distributions, shut-time distributions, open/shut correlation plots, and macroscopic current time courses expected from the fitted mechanism and compared them with the experimental observations.

The rate constant values from the fit of each set of single-channel data were used to calculate the relations between the agonist concentration and mean burst length (DC-PyPs program). The results were averaged and are displayed in Fig. 10 A. We also used the results of the fits to simulate realizations of single-channel activity (SCSIM program) shown in Fig. 10.

All data are expressed as mean ± SD of the mean, calculated from fits of three independent datasets. For the values of the estimated rate constants, we report the mean of estimates obtained from different sets and the coefficient of variation (CV) of the mean.

Online supplemental material

The SCAN, EKDIST, SCSIM, and HJCFIT programs are available as ZIP files and at http://onemol.org.uk, where they will continue to be updated. The online supplemental material is available at http://www.jgp.org/cgi/content/full/jgp.201411234/DC1.

RESULTS

Whole-cell concentration–response curve

The traces in Fig. 1 A are whole-cell currents elicited by the U-tube application of the agonist propylamine to ELIC channels expressed in a HEK293 cell (holding voltage of −30 mV). ELIC current responses activated relatively slowly and decayed quickly upon agonist removal. At propylamine concentrations >0.5 mM, currents clearly decreased after an initial peak, suggesting that ELIC desensitizes with sustained agonist application. The graph in Fig. 1 B is the concentration–response plot for propylamine, fitted with the Hill equation ($n = 4$).

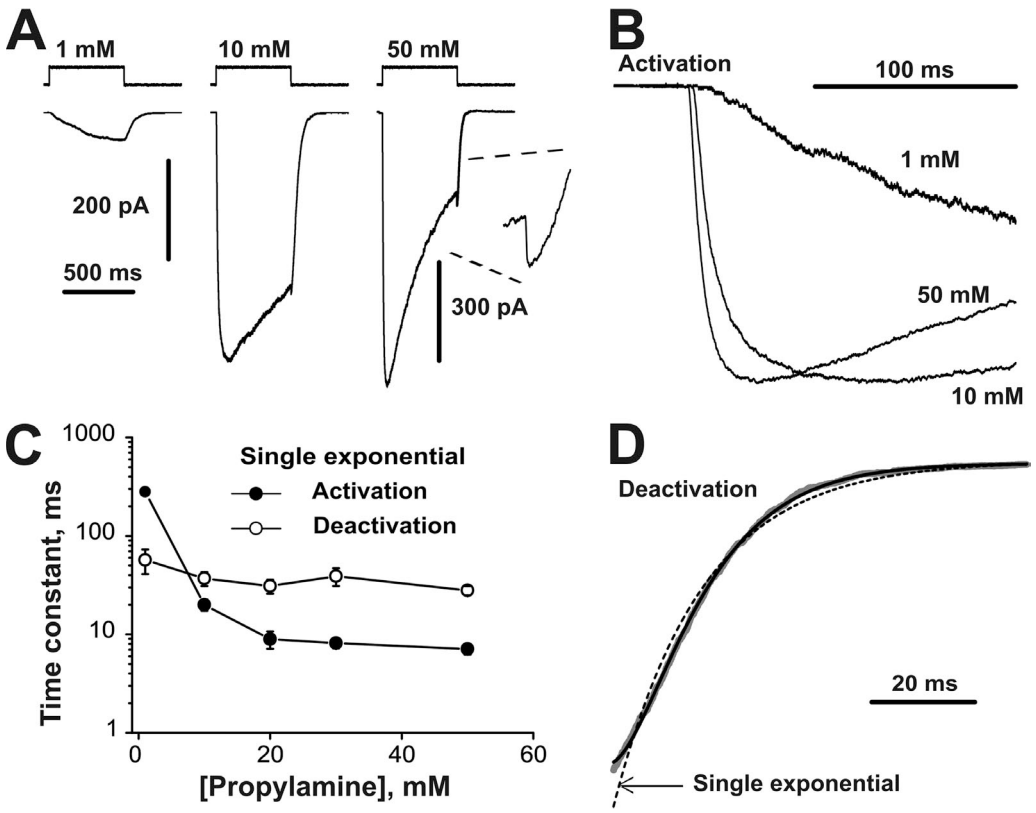

Figure 2. Macroscopic ELIC currents evoked by fast propylamine applications to outside-out patches. (A) ELIC current traces recorded in response to 500-ms steps of propylamine (the 1- and 10-mM traces are from the same patch). The enlarged inset shows the rebound current seen after the end of the propylamine pulse for concentrations >1 mM. Top traces show the solution exchange measured at the open tip at the end of each experiment. (B) The responses from A are scaled to their peak to show that the activation gets faster at higher agonist concentrations. (C) Plot of the time constants for activation and deactivation of agonist currents as a function of propylamine concentration (from fits of a single exponential; see Results; $n = 3$–7; error bars depict standard deviation of the mean). (D) This example of the deactivation phase of a response to 10 mM propylamine (gray trace) shows that the sigmoidal time course of current decay requires two exponential components for a satisfactory fit (solid black line). A single-exponential fit is shown for comparison.

Published December 29, 2014

The average EC_{50} was 500 ± 100 µM, and the Hill slope was 2.2 ± 0.1. The maximum current (9 ± 2 nA) was reached at 5 mM propylamine. These values are very similar to those reported for ELIC receptors expressed in oocytes (EC_{50} = 446 µM and Hill slope = 3.0; Zimmermann and Dutzler, 2011).

Outside-out macroscopic currents

We also recorded macroscopic currents elicited by fast, theta-tube application of propylamine onto outside-out patches to obtain a better characterization of the macroscopic time course of ELIC activation, desensitization, and deactivation. It was not possible to obtain a full dose–response curve from this set of experiments, because relatively few agonist responses could be recorded from each patch. These outside-out recordings typically lasted ∼5–10 min, and we often observed marked rundown in the amplitude of responses. Only about a quarter of patches lasted long enough to provide 10–20 agonist responses that were sufficiently stable in amplitude (<30% change) to be analyzed, and only five patches were stable enough for us to apply two different agonist concentrations.

The traces in Fig. 2 A are typical current responses to long applications of propylamine (1, 10, and 50 mM; ∼500 ms; holding voltage of −100 mV). The appearance of these responses at different agonist concentrations is very similar to that of whole-cell responses. The lowest agonist concentration at which reliable outside-out responses could be obtained was 1 mM, where currents were quite small (90 ± 50 pA; n = 4).

In Fig. 2 B, the same responses are scaled to their peak to show how their onset accelerated as the agonist concentration was increased. Current rise times were well fitted by a single-exponential component, with time constants of 280 ± 30 ms at 1 mM (n = 3), 19 ± 3 ms at 10 mM (n = 6), and 7 ± 1 ms at 50 mM propylamine (n = 7; see the plot in Fig. 2 C, closed circles).

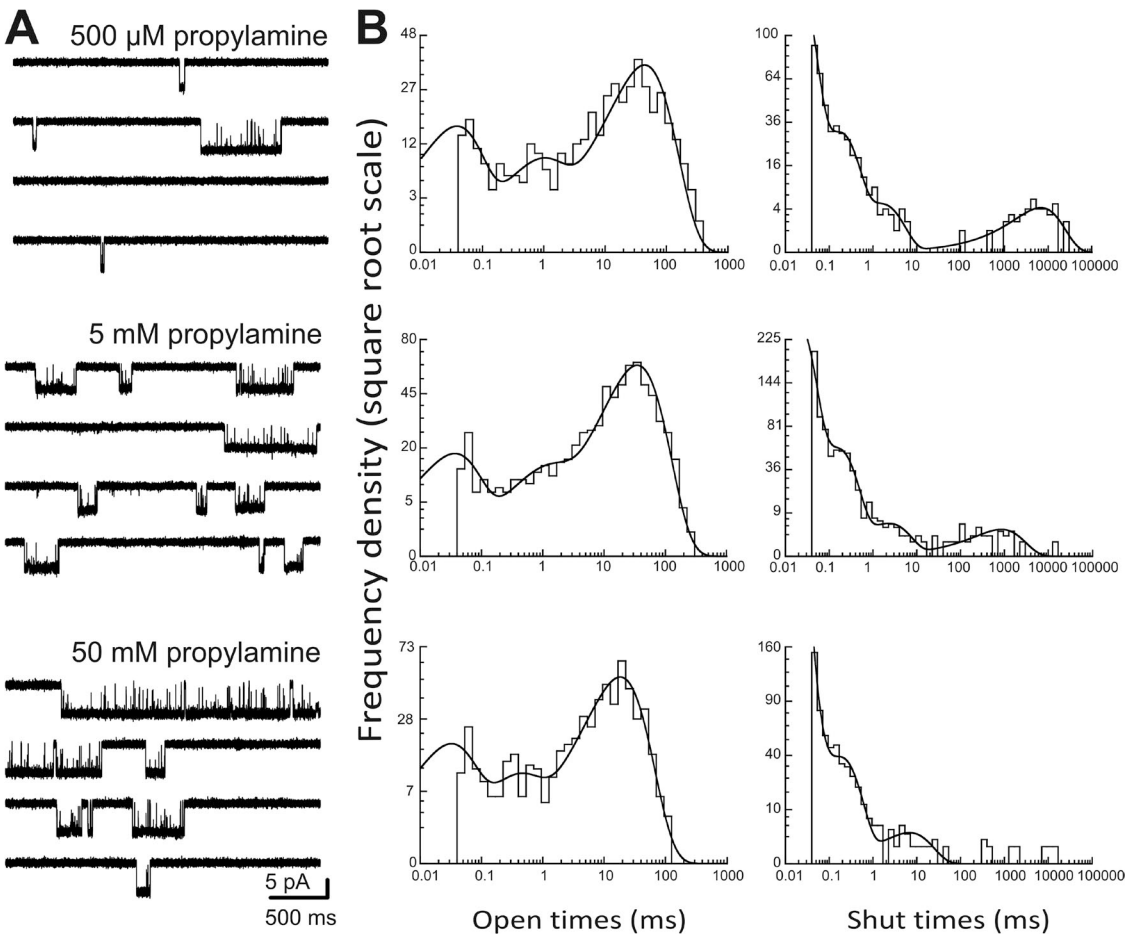

Figure 3. ELIC single-channel activity evoked by propylamine. (A) Single-channel currents in the presence of 0.5, 5, and 50 mM propylamine are shown as continuous recordings from outside-out patches held at −60 mV (filtered at 3-kHz low-pass filter for display). (B) Open- and shut-time distributions for the patches shown in A. These histograms contain all the events idealized (after imposing resolution) and are fitted with a mixture of exponential probability density functions (open times in the left column, shut times in the right column).

Published December 29, 2014

Just as in the whole-cell experiments, responses desensitized in the continuous presence of propylamine concentrations ≥10 mM and a clear sag of the current after the peak were observed in about half of the patches. At higher agonist concentrations, the decay was somewhat faster (700 ± 300 ms and 380 ± 40 ms, n = 6 and 7, at 10 and 50 mM, respectively) and the extent of desensitization was greater (residual current at 500 ms of 63 ± 7% and 34 ± 3% of peak at 10 and 50 mM propylamine, respectively).

The response deactivation that followed the end of the application was complex, regardless of agonist concentration. Fig. 2 A and its inset show that at the end of the 10- and 50-mM agonist applications, there was a rapid surge of current. The amplitude of this rebound current (expressed as a fraction of the total current at the end of the pulse, after the rebound has developed) increased with agonist concentration, and was 4.5 ± 0.3% (n = 5 out of 6 patches) and 13 ± 1% (n = 6 out of 7 patches) after 10 and 50 mM propylamine, respectively. This rebound resembles the muscle nicotinic "off" current, which is known to arise from the relief of low affinity open-channel block produced by positively charged agonists binding in the channel (Maconochie and Steinbach, 1995; Legendre et al., 2000; Lape et al., 2009).

After the rebound peak, the ELIC current decreased with a sigmoidal time course (thick gray trace in Fig. 2 D), and two exponential components with amplitudes of opposite sign were required for a good fit (Fig. 2 D, black solid line) at all agonist concentrations (including 1 mM, where the rebound current was absent). Nevertheless, we fitted the deactivation phase of the averaged currents, from 90% of the current at the end of the pulse to baseline, with a single exponential (Fig. 2 D, black dashed curve) to obtain a crude overall description of experimental deactivation and be able to compare it with the deactivation calculated from the mechanisms estimated from single-channel data (see below). The deactivation time constant (Fig. 2 C, open circles) did not change much with agonist concentration but was somewhat slower after 1 mM than after 10 mM propylamine (60 ± 20 ms vs. 30 ± 6 ms; n = 3 and 6, respectively; two-tail unpaired Student's t test; P = 0.002).

The single-channel activity of ELIC

General observations. The lowest propylamine concentration that elicited ELIC channel activity in the outside-out patch configuration was 0.3 mM. At this concentration, openings could be detected in approximately one third of the patches. Example traces of ELIC single-channel currents recorded in the presence of 0.5, 5, and 50 mM propylamine are shown in Fig. 3 A. As reported by Zimmermann and Dutzler (2011), ELIC does open to more than one conductance level. Conductance varied both within groups of openings and across different groups of openings, but differences in conductances did not occur in a clear-cut pattern. There was no obvious pattern to the occurrence of subconductances and, in particular, no relation to agonist concentration. Because of that, in the kinetic analysis we treated all conductance levels as open. In each patch that showed more than one conductance, levels were close to each other, making it hard to measure them unambiguously (by fitting Gaussians to the amplitude distribution). It was not possible to be sure that the different levels represented distinct conductance states that occurred consistently in each recording. The mean open amplitude was 8.8 ± 0.4 pA in the nine patches at 0.3–1 mM propylamine (range of 7.0–11.3 pA). Thus, in our conditions (symmetrical K^+, 0.5 mM Ba^{2+}), the chord conductance of the ELIC pore was 147 pS, much higher than the values reported

TABLE 1

Time constants and areas of the components of open- and shut-time distributions at different propylamine concentrations

Propylamine (n)	τ_1 (area [%])	τ_2 (area [%])	τ_3 (area [%])	Mean open time
mM	*ms*	*ms*	*ms*	*ms*
		Open times		
0.5 (3)	0.043 ± 0.008 (26 ± 2)	1.5 ± 0.4 (12 ± 0.5)	34 ± 6 (62 ± 3)	25 ± 5
1 (3)	0.07 ± 0.02 (20 ± 5)	5 ± 4 (13 ± 2)	39 ± 9 (68 ± 3)	30 ± 7
5 (3)	0.05 ± 0.02 (16 ± 2)	2 ± 1 (9 ± 1)	39 ± 5 (75 ± 3)	33 ± 5
10 (3)	0.04 ± 0.02 (20 ± 2)	2 ± 2 (12 ± 1)	33 ± 2 (68 ± 1)	27 ± 2
50 (3)	0.08 ± 0.03 (14 ± 5)	0.9 ± 0.3 (5 ± 3)	15 ± 2 (80 ± 9)	13 ± 2
Propylamine (n)	τ_1 (area [%])	τ_2 (area [%])	τ_3 (area [%])	τ_4 (area [%])
mM	*ms*	*ms*	*ms*	*ms*
		Shut times		
0.5 (3)	0.010 ± 0.004 (92 ± 6)	0.11 ± 0.03 (6 ± 5)	1.1 ± 0.3 (5 ± 1)	4,000 ± 2,000 (1 ± 1)
1 (3)	0.011 ± 0.003 (89 ± 9)	0.14 ± 0.03 (7 ± 6)	1.3 ± 0.3 (2 ± 2)	1,300 ± 300 (2 ± 2)
5 (3)	0.014 ± 0.004 (80 ± 12)	0.14 ± 0.02 (18 ± 10)	2.2 ± 0.2 (2 ± 1)	1,100 ± 400 (0.8 ± 0.4)
10 (3)	0.012 ± 0.002 (80 ± 8)	0.14 ± 0.02 (18 ± 7)	1.3 ± 0.4 (1.8 ± 0.4)	56 ± 4 (0.5 ± 0.3)
50 (3)	0.06 ± 0.04 (91 ± 2)	0.15 ± 0.02 (8 ± 2)	3 ± 2 (1.1 ± 0.5)	

Distributions were fitted with mixtures of exponential probability density functions. n, the number of patches for each concentration (indicated in parentheses in the first column). The time constant of each component and its relative area (in parentheses) are given as mean ± SD of the mean.

Published December 29, 2014

previously, which were measured using sodium as the permeant ion (84–96 pS; Zimmermann and Dutzler, 2011).

The off-currents observed in our macroscopic agonist responses suggest that propylamine can block the channel with low affinity. This sort of block produces shuttings that are too short to be detectable as such but should reduce the apparent amplitude of the channel openings. If present, this effect was too small to be unambiguously detected, given the observed variability in current amplitude: the average amplitude of the openings was 9.0 ± 0.75 pA and 8.2 ± 0.43 pA at 0.5 mM and 50 mM propylamine, respectively (n = 3 patches each, cf. the 13% increase in current with unblock at the end of 50-mM agonist pulses).

At first glance, ELIC resembles other ligand-gated ion channels, in that it activates in groups of openings. At 0.5 mM propylamine, the mean length of these groups of openings is 290 ± 60 ms (110 groups from three patches; critical time interval, t_{crit} of 10 ms). As the concentration increases, these groups become, on average, longer (e.g., at 5 mM propylamine, mean length is 900 ± 300 ms; 56 groups from three patches; t_{crit} of 10 ms), but medium-short groups did not entirely disappear (see the example in the bottom sweep, at 50 mM). Most other channels in the nicotinic family, except for α2 homomeric glycine receptors and 5-HT3$_A$ channels (Corradi et al., 2009; Krashia et al., 2011), respond to increases in agonist concentration with much more marked changes in behavior.

Fig. 3 B shows also the distributions for open (left column) and shut times (right), fitted with a mixture of exponential probability density functions (i.e., a sum of probability density functions, where each exponential component is weighted so that the end product is still a probability density function, e.g., has area = 1). It is of note that adequate fit of open-time distributions required three exponential components at all concentrations (see Table 1). It is very unusual for a channel in the pLGIC family to have more than one open state at saturating agonist concentrations. The values of the time constants and areas of all three components of the open-time distribution remained relatively stable in the range

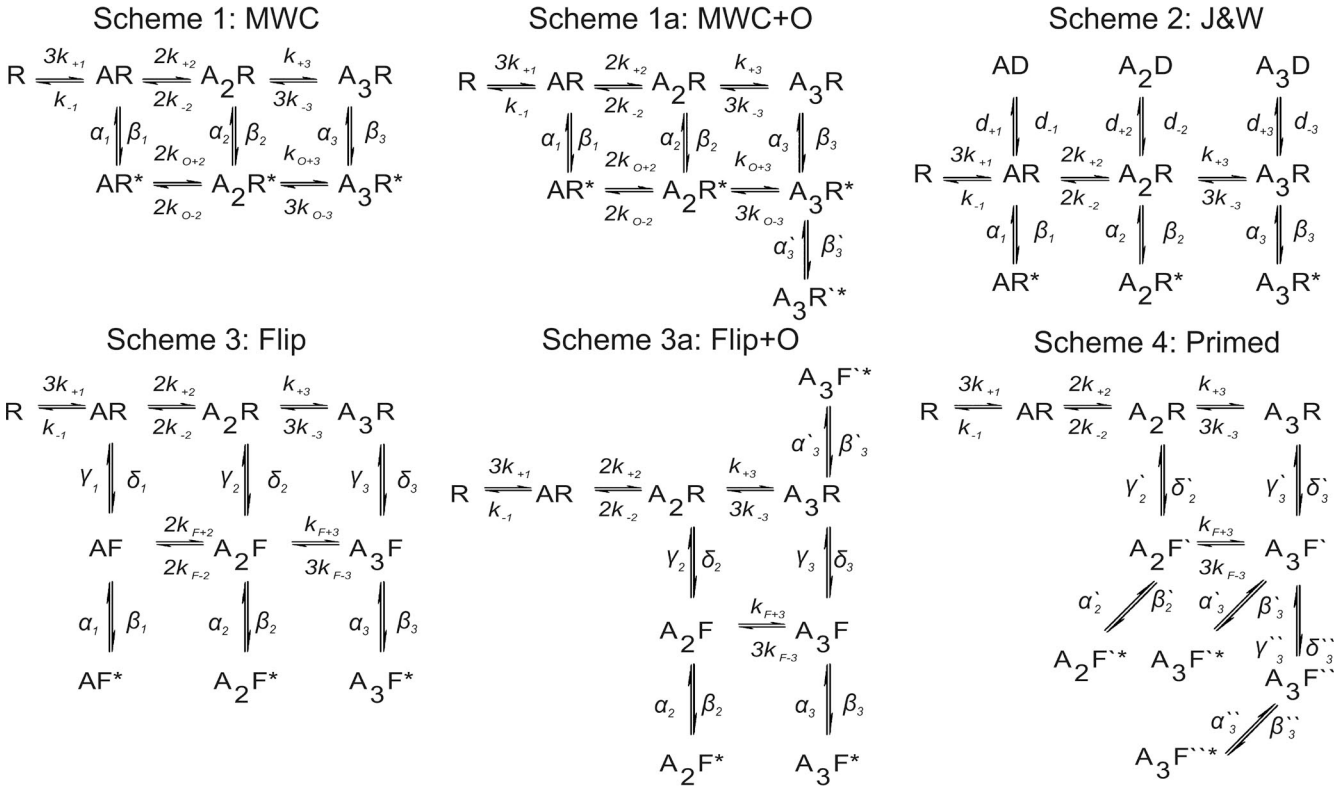

Figure 4. The main activation mechanisms tested by global fitting to ELIC single-channel data. Schemes 1–4 show the MWC mechanism, the J&W mechanism, the Flip mechanism, and a variant of the Primed mechanism as fitted, with the names of the rate constants for reference (see tables). Schemes were modified to include three binding sites and exclude unliganded openings. Schemes 1a and 3a are variants of the MWC and Flip mechanisms, modified to make an additional open state accessible to the fully liganded receptor. For the MWC mechanism, we also tested a variant where the additional open state was entered from the resting fully liganded state (not depicted). A denotes an agonist molecule, and its subscript indicates the number of agonist molecules bound to the receptor. R and R* denote resting shut states and open states of the receptor, respectively. F, F′, and F″ indicate intermediate flipped/primed shut states that connect resting and open states. In models with intermediate states, the open states are denoted by F*. D indicates distal desensitized states.

Published December 29, 2014

of propylamine concentrations tested (0.5–50 mM), except for a decline in the average duration of the longer components at 50 mM. For instance, the longest component decreased from 33 ± 2 ms at 10 mM to 15 ± 2 ms at 50 mM. Except at the highest agonist concentration, the shut-time distributions were best fitted with four exponential components (Table 1). The time constant of the slowest (fourth) component of the shut-time distribution became shorter as the agonist concentration increased, and could no longer be unambiguously detected in all patches at 50 mM propylamine.

P_{open}. At concentrations >5 mM, an additional component of very long shut intervals appeared (Fig. 3, A and B). These intervals were too few to be fitted by an exponential component, but they were clearly distinct from the next slowest shut-time component (which is concentration dependent) and were longer, ranging from 100 ms to ∼10 s. By analogy with observations in other channels (Sakmann et al., 1980), they are likely to be sojourns in long-lived desensitized states (compare the macroscopic desensitization time constant of 0.38 ± 0.04 s at 50 mM).

The presence of desensitized intervals can often be exploited in single-channel analysis to establish the concentration dependence of the P_{open} of a ligand-gated ion channel, because they divide the record into clusters of openings (see Materials and methods). If the P_{open} of these clusters is sufficiently high, clusters that show no double or multiple openings can be safely attributed to the activity of a single-channel molecule (Colquhoun and Hawkes, 1990), and the proportion of time spent in the open state measured. If entry into desensitization is sufficiently slow, each cluster contains several bursts. Bursts should become more closely spaced as agonist concentration is raised (rebinding is quicker) and cluster P_{open} increases. We attempted to identify clusters in ELIC records, namely stretches of openings that were

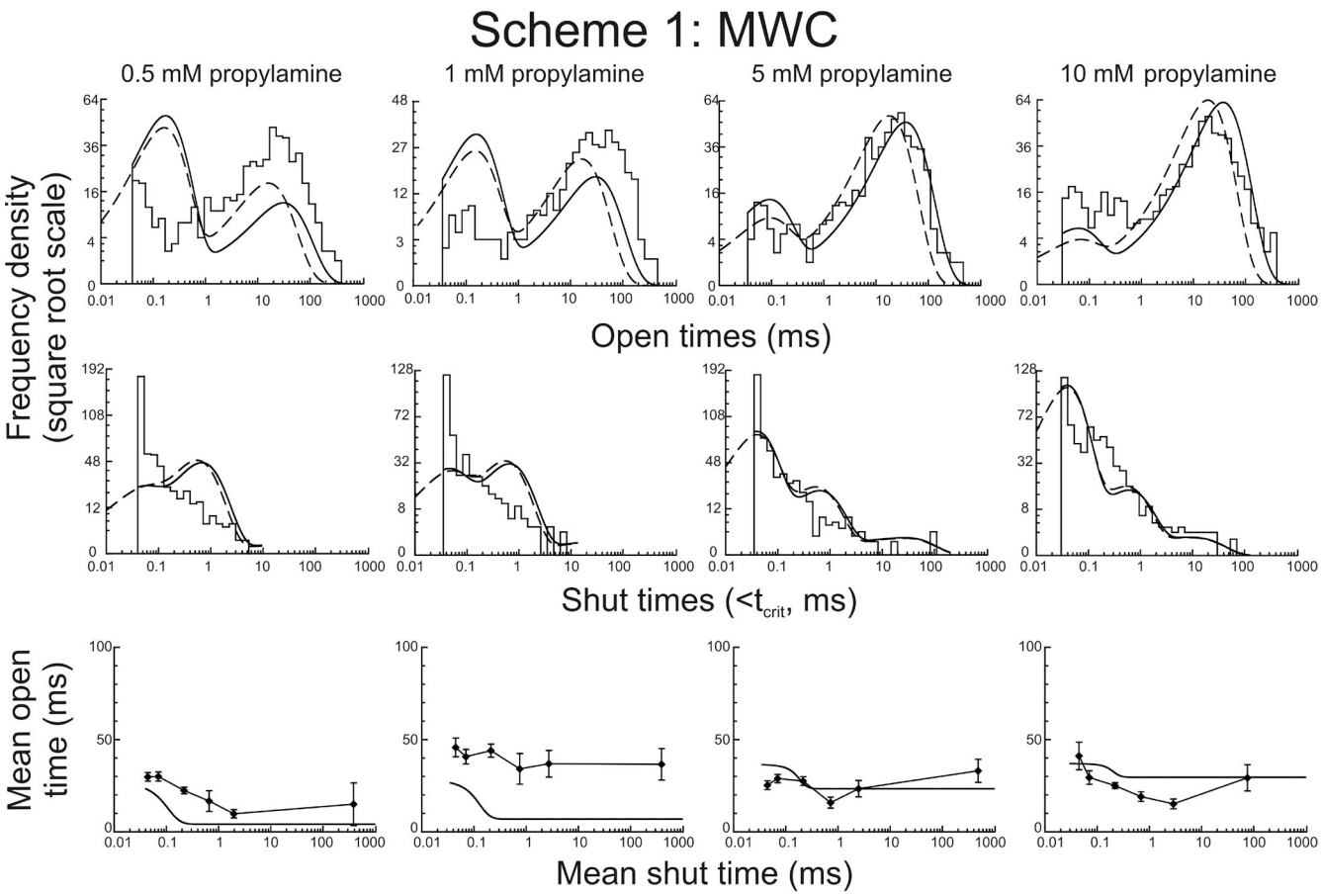

Figure 5. Testing the adequacy of the MWC mechanism fitted to ELIC single-channel data. Scheme 1 was fitted directly to a dataset of four idealized single-channel records obtained at 0.5, 1, 5, and 10 mM propylamine. The results of the fit were used to calculate the probability density functions predicted by the scheme. These are shown as solid lines in the top two rows of plots (the dashed lines are the distributions expected if there were no missed events) for open times (top) and shut times (middle). Superimposing these predicted distributions on the experimental histograms for the same records shows that the best fit of MWC does not adequately describe ELIC single-channel kinetics. The bottom-row plots compare the experimental open–shut time correlations in the records of this set (circles, error bars depicting standard deviation of the mean, and connecting lines) and the MWC scheme predictions of these correlations, calculated from the fitted rate constants (solid lines).

Published December 29, 2014

terminated by long shut intervals and were without double openings. Typically, we had very few of these long shut intervals in each patch and very few possible clusters (3–11). The choice of what to classify as an intercluster shut time was largely arbitrary, because we could not use any formal criteria to identify them (e.g., calculate a critical time interval between two exponential components to minimize misclassified shut-interval number). We chose an arbitrary critical time interval, t_{crit}, so that the longest well-defined exponential component in the shut-time distributions was interpreted as arising within the cluster (as suggested by its dependence on concentration). By this criterion, gaps were classified as between clusters if longer than 100 ms at 10 mM, 50 ms at 50 mM, and 10 ms at 100 mM. Cluster P_{open} values were calculated for all of these concentrations and were found to be similar and >96%. Note that the macroscopic dose–response curve of Fig. 1 indicates that concentrations ≥5 mM should elicit a maximum receptor response. At concentrations <10 mM, we could not identify desensitized gaps, and therefore we were unable to define clusters to construct a P_{open} curve.

Fitting activation mechanisms to single-channel data

We investigated the activation process of the ELIC receptor by fitting a range of mechanisms directly to the single-channel data, using the HJCFIT program. Candidate activation mechanisms were fitted to three independent sets of single-channel data. Each set contained four records obtained at different propylamine concentrations (0.5, 1, 5, and 10 mM) spanning the whole of the dose–response curve, to obtain sufficient information on the different steps of the mechanism. Each single-channel record was appropriately divided into bursts or clusters (see Materials and methods and Colquhoun et al., 2003).

The adequacy of the models fitted was judged by comparing their predictions with the experimental observations. The rate constant values estimated in the fits were used to calculate the expected appearance of several types of single-channel data displays (i.e., open- and shut-time distributions and open- and shut-time correlations) and the time course of macroscopic current responses to fast concentration jumps.

We tested several kinetic mechanisms belonging to four major classes of models (Fig. 4) that have been successfully used to investigate the activity of channels in the pLGIC family, namely, "Monod–Wyman–Changeux" (MWC; Scheme 1), "Jones and Westbrook" (J&W; Scheme 2), "Flip" (Scheme 3), and "Primed" (Scheme 4). Note that the P_{open} of unliganded wild-type ELIC is too low for us to obtain information on unliganded openings, and therefore unliganded open states (which would be denoted "R*") are neither shown in the mechanisms in Fig. 4 nor fitted.

TABLE 2

Rate and equilibrium constant values obtained from the global fits of MWC and MWC + Open models to single-channel data sets

Rate and equilibrium constants	Unit	MWC (Scheme 1)	MWC + Open (Scheme 1a)
α_3'	s^{-1}		167 ± 9%
β_3'	s^{-1}		6,450 ± 14%
α_1	s^{-1}	60 ± 63%	86,300 ± 100%
β_1	s^{-1}	0.147 ± 71%	7 ± 100%
α_2	s^{-1}	3,150 ± 27%	101,200 ± 49%
β_2	s^{-1}	2,730 ± 10%	5,480 ± 68%
α_3	s^{-1}	46 ± 7%	2,100 ± 16%
β_3	s^{-1}	31,400 ± 5%	15,300 ± 32%
k_+	$M^{-1}\,s^{-1}$	2.54×10^4 ± 10%	2.15×10^4 ± 67%
k_-	s^{-1}	163 ± 7%	58 ± 63%
k_{o+}	$M^{-1}\,s^{-1}$	1.40×10^6 ± 24%	9.97×10^7 ± 96%
k_{o-}	s^{-1}	13.3 ± 41%	93 ± 51%
$E_1 = \beta_1/\alpha_1$		0.0016 ± 42%	0.0002 ± 82%
$E_2 = \beta_2/\alpha_2$		1.0 ± 29%	0.04 ± 69%
$E_3 = \beta_3/\alpha_3$		700 ± 11%	7.9 ± 35%
$E_3' = \beta_3'/\alpha_3'$			38.6 ± 11%
$K_R = k_-/k_+$	mM	6.4 ± 5%	6.3 ± 11%
$K_o = k_{o-}/k_{o+}$	mM	0.0092 ± 24%	22.9 ± 64%
EC_{50}	mM	0.81 ± 3%	1.14 ± 6%
n_H		2.6 ± 1%	2.5 ± 2%

The fits constrain the binding and unbinding rates to be the same, regardless of the number of molecules bound and the conformation. Those constraints were implemented by the following equations: $k_{+1} = k_{+2} = k_{+3} = k_+$; $k_{-1} = k_{-2} = k_{-3} = k_-$ and $k_{o+2} = k_{o+3} = k_{o+}$; $k_{o-2} = k_{o-3} = k_{o-}$. In addition, one rate constant in each cycle was fixed by the constraint of microscopic reversibility (Colquhoun et al., 2004). The equilibrium constants, E and K, and the values for the EC_{50} and Hill slope (n_H) of the predicted P_{open} curve were calculated from the rate constants for each set and then averaged. Values are means ± coefficient of variation (i.e., SD of the mean expressed as a percentage of the mean).

Published December 29, 2014

Scheme 1: MWC model (Fig. 4 A). MWC is an adaptation of the model proposed by Monod, Wyman, and Changeux in 1965 for the functional properties of allosteric proteins (Monod et al., 1965). The MWC mechanism has been widely used to describe the activation of many ion channels. In particular, it has been used for energy calculations in another member of the Cys-loop family, the muscle nicotinic acetylcholine receptor (Auerbach, 2012). The MWC mechanism postulates that the channel can reversibly adopt two global conformational states, open or closed, and that these two conformations have different affinities for the ligand. This implies that the agonist-binding sites are independent, and that the binding affinity depends on the state of the receptor (e.g., open or closed), but not on the level of ligation. When fitting a mechanism to data, this means imposing the constraint that the microscopic-binding rate constants should be the same at each level of ligation: $k_{+1} = k_{+2} = k_{+3} = k_+$, $k_{-1} = k_{-2} = k_{-3} = k_-$. In the MWC variant used here, three molecules of agonist can bind, and there are three cycles and eight free parameters (plus three rate constants calculated from microscopic reversibility).

Examples of open- and shut-time distributions and correlation plots for one of the fitted sets are shown in Fig. 5. The top and middle rows are the predictions from the fit (solid smooth line) superimposed on the open- and shut-time experimental histograms. Even a cursory inspection of the open- and shut-time distributions is sufficient to see that the predictions of this scheme were very poor at all concentrations.

Of course it is not surprising that a scheme such as MWC, with a single fully liganded open state, should fail to describe an open-time distribution that has more than one open component at high agonist concentration. The simplest explanation of this behavior is that the fully bound channel can open to more than one open state. In an effort to improve fits, we tried variants of the MWC mechanism with extra open states connected either to A_3R^* (e.g., Scheme 1a in Fig. 4; fit results summarized in Table 2) or to A_3R (not depicted). These variants were better at predicting open- but not shut-time distributions (not depicted). To improve the prediction of shut times, we also ran fits of the two variants of MWC without the constraint of microscopic reversibility, or with different statistical factors for binding (e.g., assuming that five sites are initially available for binding), but none of these attempts produced any improvement (not depicted). Thus, we proceeded to test mechanisms with more shut states, from different mechanism classes (Fig. 4).

Scheme 2: J&W mechanism. One such scheme is the J&W mechanism (Scheme 2 in Fig. 4; Jones and Westbrook, 1995), which postulates that when the receptor is in one of the resting bound states, it can either open or enter a short-lived desensitized state. The J&W scheme was fitted to ELIC data without constraints on the binding rate constants, because in other channels in this superfamily, J&W-type schemes fit well only if the agonist-binding sites were allowed to interact with each other, and change their affinity with the level of ligation. The number of free parameters was 18 (Table 3).

The prediction of shut-time distributions was slightly better with J&W than with MWC, in part, no doubt, because the J&W mechanism has more shut states and more free parameters. As with MWC, this form of J&W has only one fully liganded open state, and its prediction of open-time distributions was very poor (not depicted). This was substantially improved by adding extra open states to the fully liganded branch (e.g., connected to the A_3R^* state; not depicted). Even so, the rate constant estimates from J&W were very variable across the three independent datasets analyzed.

TABLE 3

Rate and equilibrium constant values obtained from the global fits of the J&W model to three independent single-channel data sets

Rate and equilibrium constants	Unit	J&W
α_1	s^{-1}	86,300 ± 100%
β_1	s^{-1}	16 ± 64%
α_2	s^{-1}	14,900 ± 41%
β_2	s^{-1}	37,400 ± 93%
α_3	s^{-1}	127 ± 13%
β_3	s^{-1}	56,600 ± 6%
d_{-1}	s^{-1}	12,400 ± 100%
d_{+1}	s^{-1}	336,000 ± 99%
d_{-2}	s^{-1}	4,680 ± 75%
d_{+2}	s^{-1}	1,730 ± 19%
d_{-3}	s^{-1}	5,460 ± 18%
d_{+3}	s^{-1}	6,010 ± 20%
k_{-1}	s^{-1}	378,000 ± 83%
k_{+1}	$M^{-1}\,s^{-1}$	6.88×10^5 ± 52%
k_{-2}	s^{-1}	476 ± 7%
k_{+2}	$M^{-1}\,s^{-1}$	3.78×10^5 ± 5%
k_{-3}	s^{-1}	112,000 ± 99%
k_{+3}	$M^{-1}\,s^{-1}$	1.08×10^8 ± 99%
$E_1 = \beta_1/\alpha_1$		0.37 ± 99%
$E_2 = \beta_2/\alpha_2$		1.5 ± 81%
$E_3 = \beta_3/\alpha_3$		450 ± 8%
$K_1 = k_{-1}/k_{+1}$	mM	1,500 ± 62%
$K_2 = k_{-2}/k_{+2}$	mM	1.3 ± 8%
$K_3 = k_{-3}/k_{+3}$	mM	1.3 ± 12%
$D_1 = d_{+1}/d_{-1}$		210 ± 74%
$D_2 = d_{+2}/d_{-2}$		0.99 ± 45%
$D_3 = d_{+3}/d_{-3}$		1.3 ± 41%
EC_{50}	mM	1.9 ± 43%
n_H		2.3 ± 10%

All of the rate constants were fitted freely in HJCFIT. The values for efficacy at each level of ligation, E, the microscopic dissociation equilibrium constants per site, K, the equilibrium constants for the entry into the extra shut states, D_n, the EC_{50} and the Hill slope for the P_{open} curve were calculated from the rate constants for each set, and their means are listed at the bottom of the table. Values are means ± coefficient of variation (i.e., SD of the mean expressed as a percentage of the mean).

Published December 29, 2014

Scheme 3: "Flip" mechanism. The Flip mechanism (Scheme 3 in Fig. 4) describes well the single-channel activity of several glycine receptor isoforms (Burzomato et al., 2004; Lape et al., 2008; Krashia et al., 2011; Marabelli et al., 2013). This scheme postulates the existence of an additional set of shut ("flipped") states that represent a concerted conformational change that occurs before the channel opens (Burzomato et al., 2004; Sivilotti, 2010). Scheme 3 has three open states and three flipped states, one at each level of ligation. In Flip-type models, the agonist-binding sites are independent and, as in MWC, the binding affinity depends only on the state of the receptor (i.e., resting or flipped), and not on the level of ligation. Hence, the scheme estimates only two equilibrium constants for binding—one for the resting conformation (R) and one for the flipped conformation (F)—regardless of how many sites are already occupied. This is done by applying the following constraints to the binding rate constants: $k_{+1} = k_{+2} = k_{+3} = k_{+}$, $k_{-1} = k_{-2} = k_{-3} = k_{-}$, $k_{F+2} = k_{F+3} = k_{F+}$ and $k_{F-2} = k_{F-3} = k_{F-}$. In addition to that, two rate constants (δ_1 and δ_3, mono- and triliganded unflipping) are constrained by the requirement of microscopic reversibility for the two cycles (Colquhoun et al., 2004), and therefore this mechanism had only 14 free parameters.

Open-/shut-time distributions and correlation plots for the example set fitted with Scheme 3 are shown in Fig. 6. The average values for the rate constants estimated for all three sets are shown in Table 4. Just as we found for the MWC and the J&W models, Flip, with a single fully liganded open state, could not describe ELIC open-time distributions. The shut-time distributions and the correlation plots predicted by fits of the Flip and J&W mechanisms were almost indistinguishable.

Again, we also tested Flip scheme variants, with an extra open state connected to one of the fully liganded states. The best of these was Scheme 3a (Fig. 4; results shown in Fig. 7 and Table 4). This was the first mechanism to provide an adequate description of the data, as shown by the open- and shut-time distributions in Fig. 7. The flipped intermediate states are reached more easily as more binding sites are occupied and the flipping equilibrium constant, *F*, increases from 0.1 (flipping from A_2R) to 0.4 (flipping from A_3R; cf. values of 1 and 8 for the same steps in the α1 homomeric glycine receptor, Burzomato et al., 2004). The ELIC values are low, suggesting that the

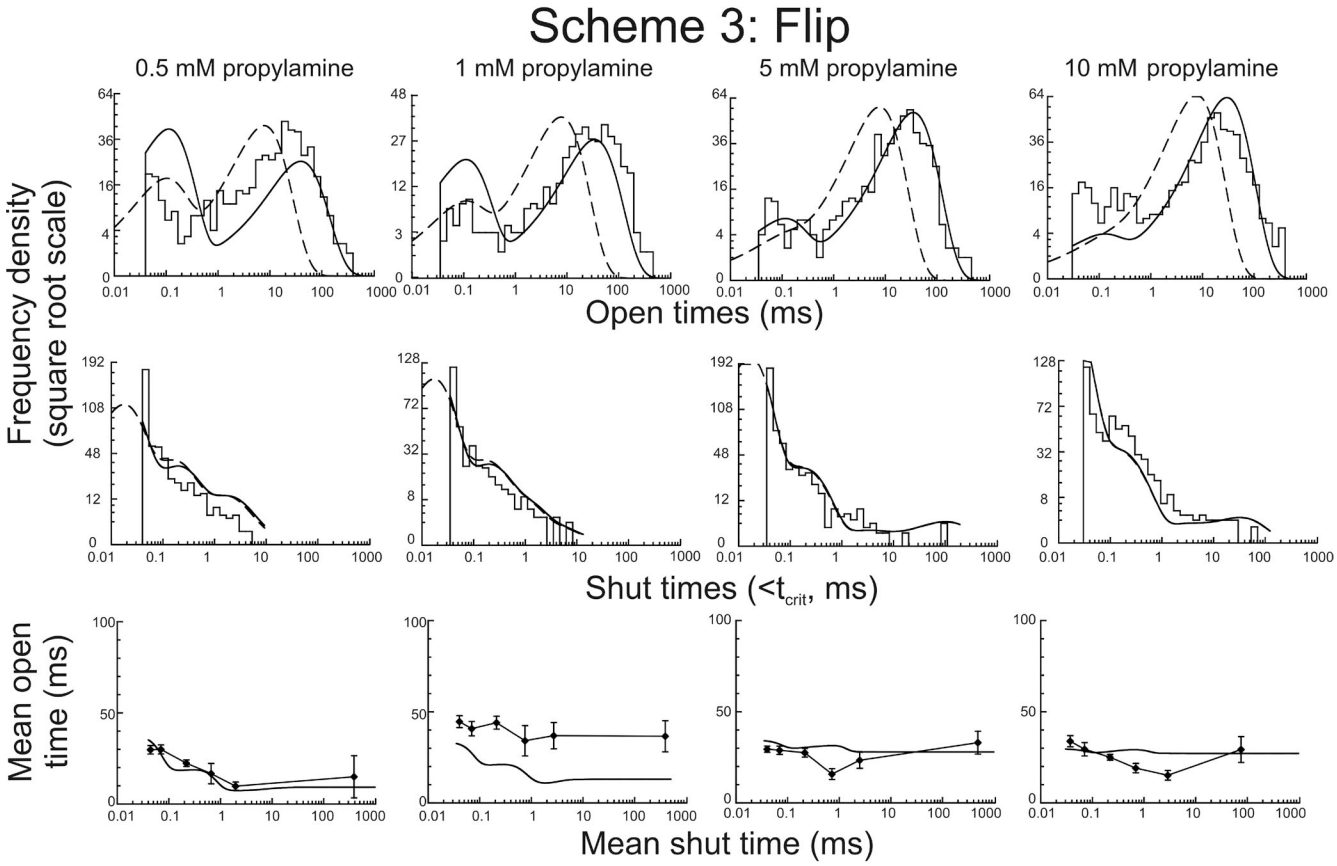

Figure 6. Testing the Flip mechanism fitted to ELIC single-channel data. The plots compare the experimental results (open- and shut-time distributions and open–shut correlations; see details in the legend of Fig. 5; error bars depict standard deviation of the mean) with the predictions of the fit of Scheme 3, Flip, fitted to the same dataset as in Fig. 5. The Flip mechanism was no better than MWC at describing open-time distributions, but its prediction of the shut-time distribution was better.

Published December 29, 2014

initial conformational change is relatively unfavorable in ELIC compared with other nicotinic-type channels. Note also that for ELIC we could not get consistent estimates for the monoliganded flipping and opening steps (probably because transitions do not occur often enough), and thus Scheme 3a does not attempt to include such states in the fit. The main open state for fully liganded ELIC is reached with high opening efficacy (E_3 = 510), which is largely caused by a low closing rate constant (120 s^{-1}). Doubly liganded channels that have flipped can also open, with fairly high opening efficacy (E_2 = 21). The increase in the propylamine affinity for the binding site with flipping was about fivefold (going from a resting value K_R = 6.9 mM to a flipped value K_F = 1.3 mM), in line with the relatively modest value estimated for α1 homomeric glycine receptors.

Scheme 4: Primed mechanism. Fully liganded opening to more than one open state is an intrinsic property of the Primed class of mechanisms (Mukhtasimova et al., 2009). These postulate that channel subunits or binding sites change conformation independently of each other, rather than in a concerted fashion (as in Flip), and that the channel can open from any (of several) preopening intermediates. We showed that this feature is necessary to describe the behavior of a startle disease mutant form of the glycine receptor, α1K276Eβ (Lape et al., 2012).

The general form of the Primed mechanism with three binding sites has too many free parameters for robust estimation, but we obtained a good fit with the reduced Primed mechanism shown as Scheme 4 in Fig. 4. The scheme has three open states and two primed states, which are accessible from the di- and triliganded resting

TABLE 4

Rate and equilibrium constant values obtained from the global fits of the Flip and Flip + Open to three independent single-channel data sets

Rate and equilibrium constants	Unit	Flip (Scheme 3)	Flip + Open (Scheme 3a)
α'_3	s^{-1}		19,200 ± 21%
β'_3	s^{-1}		1,590 ± 16%
α_1	s^{-1}	21,000 ± 99%	
β_1	s^{-1}	24,000 ± 67%	
α_2	s^{-1}	31,000 ± 62%	12,000 ± 48%
β_2	s^{-1}	124,000 ± 55%	125,000 ± 5%
α_3	s^{-1}	88 ± 24%	120 ± 18%
β_3	s^{-1}	37,600 ± 23%	61,600 ± 22%
γ_1	s^{-1}	0.0491 ± 81%	
δ_1	s^{-1}	0.00014 ± 90%	
γ_2	s^{-1}	3,260 ± 46%	758 ± 48%
δ_2	s^{-1}	421 ± 84%	87 ± 81%
γ_3	s^{-1}	5,920 ± 31%	10,900 ± 10%
δ_3	s^{-1}	6,820 ± 28%	4,580 ± 18%
k_-	s^{-1}	156 ± 26%	158 ± 9%
k_+	$M^{-1}\,s^{-1}$	1.14×10^4 ± 14%	2.97×10^4 ± 38%
k_{f-}	s^{-1}	175,000 ± 93%	44,400 ± 9%
k_{f+}	$M^{-1}\,s^{-1}$	5.23×10^8 ± 98%	7.35×10^7 ± 72%
$E_{3R} = \beta_{3R}/\alpha_{3R}$			0.085 ± 5%
$E_1 = \beta_1/\alpha_1$		130 ± 54%	
$E_2 = \beta_2/\alpha_2$		4.7 ± 62%	21 ± 58%
$E_3 = \beta_3/\alpha_3$		430 ± 4%	507 ± 4%
$F_1 = \delta_1/\gamma_1$		0.0048 ± 55%	
$F_2 = \delta_2/\gamma_2$		0.088 ± 55%	0.10 ± 60%
$F_3 = \delta_3/\gamma_3$		1.6 ± 55%	0.41 ± 8%
$K_R = k_-/k_+$	mM	15 ± 31%	6.9 ± 36%
$K_f = k_{f-}/k_{f+}$	mM	0.81 ± 31%	1.3 ± 36%
E_{eff}		230 ± 27%	150 ± 10%
EC_{50}	mM	1.37 ± 15%	1.40 ± 39%
n_H		2.43 ± 1%	2.35 ± 5%

The fits assume that the binding sites are equivalent and independent and therefore constrain the binding and unbinding rates to be the same if the conformation is the same, regardless of the number of molecules bound. This constraint was implemented by the following equations: $k_{+1} = k_{+2} = k_{+3} = k_+$; $k_{-1} = k_{-2} = k_{-3} = k$, and $k_{f+1} = k_{f+2} = k_{f+3} = k_{f+}$; $k_{f-2} = k_{f-3} = k_{f-}$. In addition, one rate constant in each cycle was fixed by the constraint of microscopic reversibility (Colquhoun et al., 2004). The equilibrium constants *E*, *F*, and *K*, effective efficacy, E_{eff}, and the EC_{50} and Hill slope values for the P_{open} curve were calculated from the rate constants for each set and then averaged. Values are means ± coefficient of variation (i.e., SD of the mean expressed as a percentage of the mean).

Published December 29, 2014

states. This mechanism has 15 free parameters, the agonist-binding sites are independent, and binding affinity depends only on the state of the receptor (i.e., resting, R, or primed, F′), regardless of how many sites are already occupied. In addition, one rate constant (δ'_2) was constrained by microscopic reversibility (Colquhoun et al., 2004).

The results of fitting this scheme are summarized in Fig. 8 and Table 5. The prediction of both open- and shut-time distributions and open–shut correlations was good at all agonist concentrations. Furthermore, parameter estimates were much more consistent across sets for the Primed mechanism than with other mechanisms. As more agonist molecules bind, activated states become more accessible. This is largely an effect of easier priming, as the value of the priming equilibrium constant, F, increased from 0.013 (A_2R priming to A_2F') to 0.76 and 0.72 (A_3R priming to A_3F' and A_3F' priming to A_3F'', respectively). The most effective opening occurs from the highest primed fully bound state (A_3F''), with a very high opening equilibrium constant ($E_3'' = 450$), an opening rate constant of 72,000 s^{-1}, and a closing rate constant of 180 s^{-1}. As in the modified Flip mechanism, partially bound (diliganded) channels open with relatively high efficacy, once they have reached the primed state, as E_2' is 97. The increase in propylamine affinity with priming was 50-fold ($K_R = 7.1$ mM and $K_F = 0.14$ mM). An equally good prediction of the open- and shut-time distributions was obtained with a Primed mechanism with two, rather than three, binding steps, and three open states (parameter estimates were not substantially different; see Table 5).

Prediction of P_{open} and macroscopic channel behavior

We found that only the modified Flip and the Primed mechanisms could describe the ELIC single-channel open-/shut-time distributions. Can these schemes also account for the other experimental observations we obtained?

Maximum P_{open} is given by

$$Max\ P_{open} = \frac{E_{eff}}{E_{eff} + 1}, \quad (1)$$

where E_{eff} is the overall agonist efficacy.

In the Flip + Open scheme, E_{eff} depends on the equilibrium constant for flipping (F_3) and the equilibrium

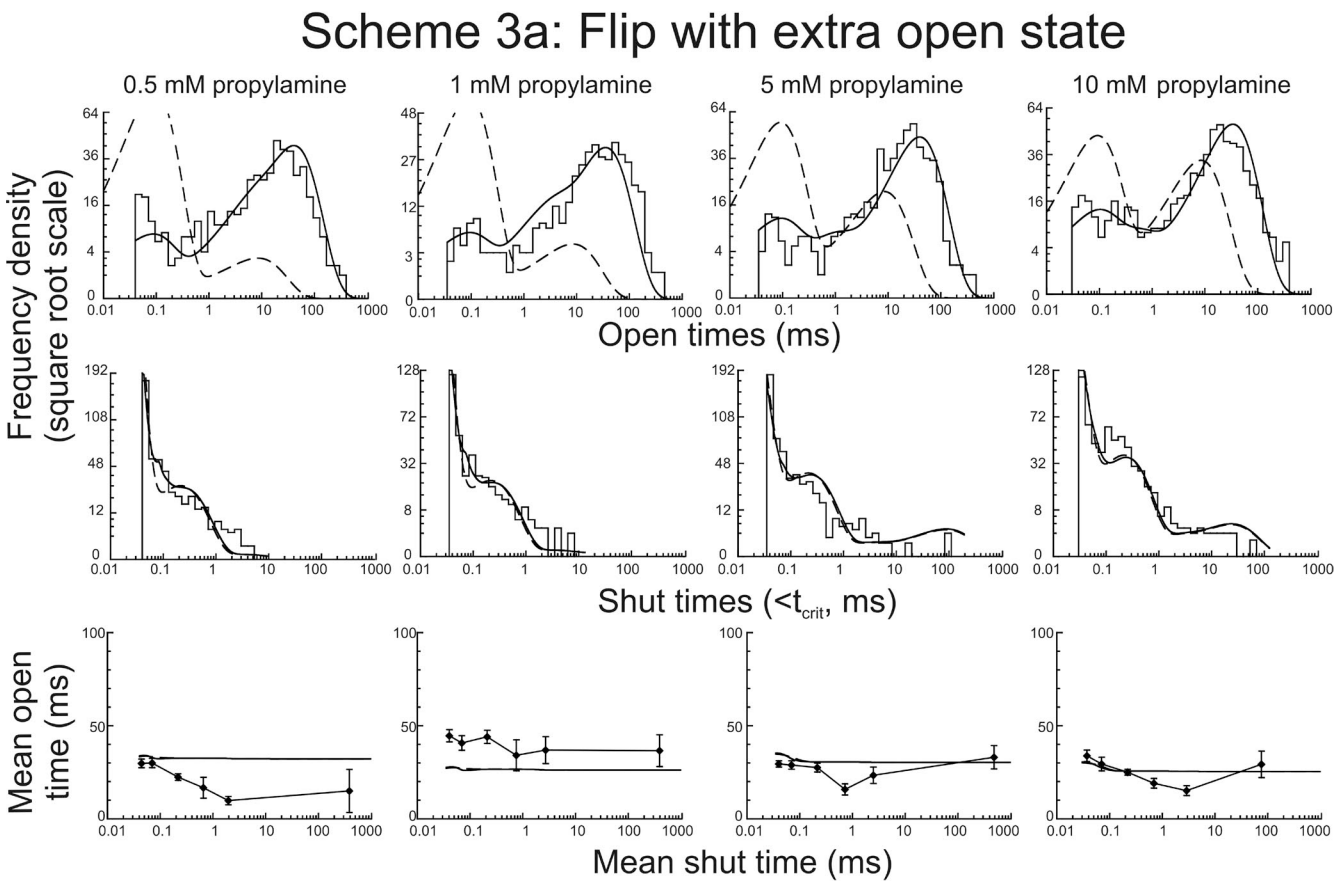

Figure 7. Testing Flip + O, a variant of the Flip mechanism with an added open state, fitted to ELIC single-channel currents. As in Fig. 5, the plots compare the experimental open- and shut-time distributions and correlations with those calculated from the results of fitting Flip + O (Scheme 3a in Fig. 4) to the same dataset as in Fig. 5 (error bars depict standard deviation of the mean). Note that open-time distributions were predicted well when an extra open state was added to the fully liganded end of Flip.

Published December 29, 2014

constants for opening (E_{3R} and E_3) for the fully liganded receptor:

$$E_{eff} = \frac{E_{3R} + E_3 F_3}{F_3 + 1}. \quad (2)$$

In the Primed scheme, E_{eff} depends on the equilibrium constant for Primed (F' and F'') and the equilibrium constant (E' and E'') for the open–shut reaction for the fully liganded receptor:

$$E_{eff} = \frac{E_3' F_3' + E_3'' F_3'' F_3'}{F_3' F_3'' + F_3' + 1}. \quad (3)$$

The effective efficacy for propylamine on ELIC was very high in both schemes: 150 in Flip + Open and 102 in Primed.

Both schemes predicted a maximum P_{open} >99%, to be compared with our observations of average cluster P_{open} values of 96.3 ± 0.8% at 50–100 mM propylamine.

Because we could not obtain a single-channel concentration–P_{open} curve, we can compare mechanism predictions only with our whole-cell dose–response curves, from which no absolute values of P_{open} can be inferred. Both single-channel schemes predicted for the propylamine P_{open} curve an EC_{50} of 1.4 mM, somewhat higher than the observed value of 0.5 mM (Tables 4 and 5). The value of this comparison is limited, because the single-channel mechanisms are estimated from data from which desensitized intervals are excluded, whereas whole-cell dose–response curves may well be affected by desensitization, because of the relative slowness of agonist applications in these experiments. In principle, partial equilibration with desensitized states (which are by definition high affinity) at the response peak should increase the apparent agonist potency and thus may account for some of this discrepancy.

Another feature of the macroscopic dose–response curve that we must compare with model schemes is the Hill slope. Both the Flip and the Primed schemes with three agonist-binding sites predicted Hill slopes of 2.35–2.50 (cf. the observed n_H value of 2.2), whereas the Primed scheme with two binding sites predicted an n_H of 1.84. However, the slope of the macroscopic dose–response curve is likely to be affected by the low affinity agonist block of the channel, which is not included in the mechanisms fitted. Therefore, we recalculated the P_{open}

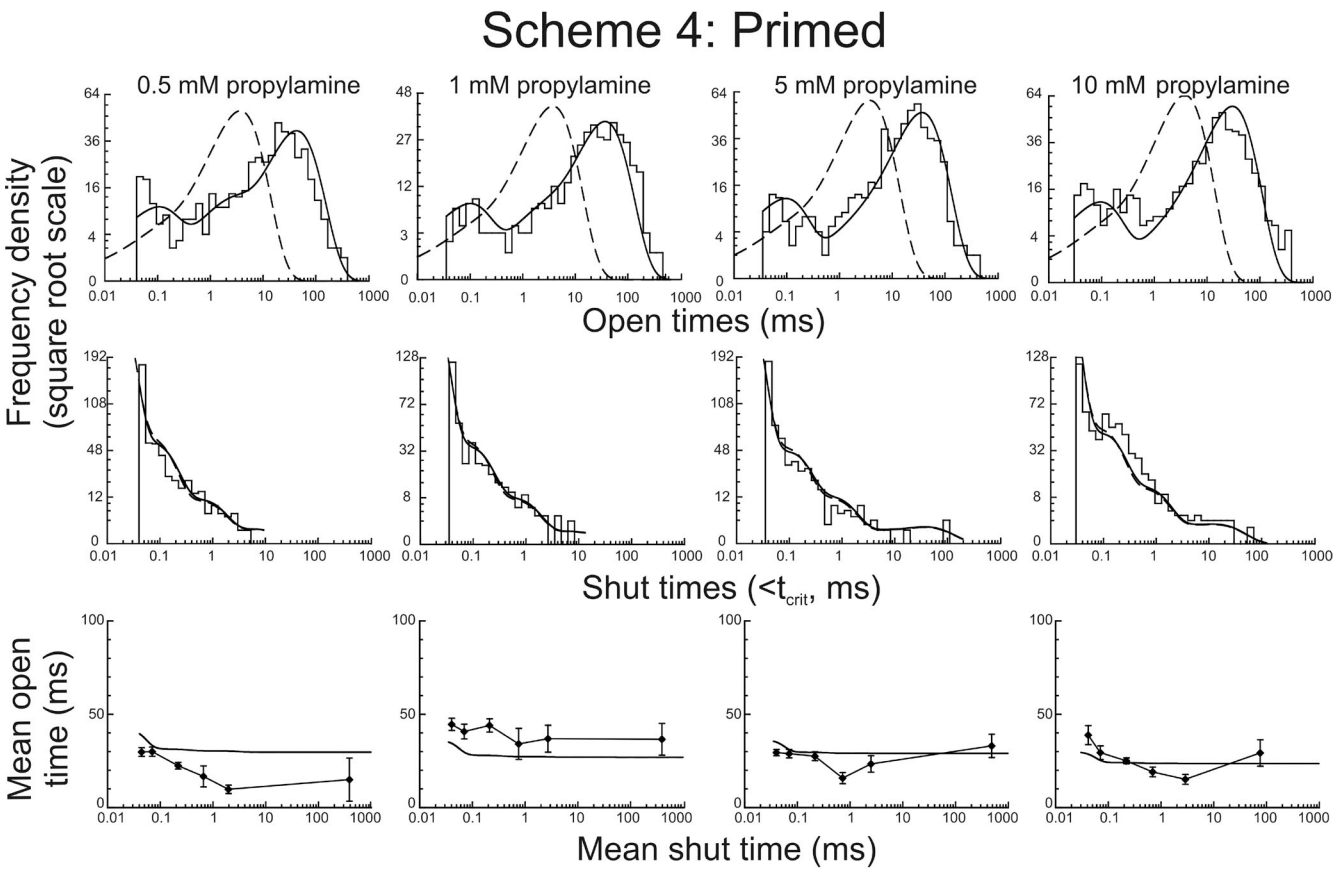

Figure 8. Fits of a Primed-type mechanism to ELIC single-channel currents. The results of fitting Scheme 4 (primed, three binding sites; see Fig. 4) are shown by the plots, as comparisons of the scheme predictions with the experimental open- and shut-time distributions and open–shut correlations. Same dataset and details as in Fig. 5 (error bars are standard deviation of the mean). The Primed mechanism allows the channel to enter more than one "layer" of intermediate states before opening, and provided a good description for all the single-channel observables. Similar results were obtained by fitting the Primed scheme with two binding sites.

Published December 29, 2014

curves predicted by the Primed mechanisms with two and three binding sites, after incorporating fast-equilibrating open-channel block, with a propylamine block dissociation constant of 460 mM (estimated by fitting the concentration dependence of the rebound current at the end of propylamine jumps). Distinguishing between two and three binding sites on the basis of these results is not easy. For the two-site scheme, correction for block improved the predicted Hill slope (increasing it to 1.98 ± 0.06) but deteriorated the prediction of maximum P_{open} to 91.3 ± 3%. Conversely, for the three-site scheme with block, the prediction of the Hill slope was worse (2.63 ± 0.01), but that of the maximum P_{open} remained adequate at 94.1 ± 0.2%. The greater reliability of the maximum P_{open} measurements would suggest giving the preference to the three-site scheme, but the difference is marginal.

We also calculated the predictions of the Flip and Primed schemes with three binding sites for the time course of agonist outside-out currents. A recorded macroscopic current response to a 500-ms, 10-mM propylamine pulse is shown in Fig. 9 A, and the equivalent response calculated, for a realistic agonist pulse, with the Primed mechanism (Scheme 4, three binding sites) is shown in Fig. 9 B. This first calculated response does not decline during the application, because the single-channel analysis does not attempt to estimate desensitization, but desensitized states can be added empirically to the mechanism to give Scheme 4 (three sites) + D in Fig. 9 C. We chose a value of 1 s^{-1} for the forward rate constant (into desensitization) to match the reciprocals of the approximate cluster length and of the macroscopic desensitization τ, and a value of 0.5 s^{-1} for the backward rate constant (out of desensitization) to reproduce the observed extent of desensitization at the end of this pulse. The macroscopic current calculated from this variant of the Primed scheme for the same agonist pulse (three binding

TABLE 5

Rate and equilibrium constant values obtained from the global fit of the Primed model (with two or three binding steps) to three independent single-channel data sets

Rate and equilibrium constants	Unit	Primed (two binding sites)	Rate and equilibrium constants	Unit	Primed (three binding sites)
α''_2	s^{-1}	174 ± 26%	α''_3	s^{-1}	176 ± 26%
β''_2	s^{-1}	71,400 ± 11%	β''_3	s^{-1}	72,200 ± 11%
α'_2	s^{-1}	12,700 ± 3%	α'_3	s^{-1}	12,700 ± 3%
β'_2	s^{-1}	3,310 ± 28%	β'_3	s^{-1}	3,430 ± 28%
α'_1	s^{-1}	661 ± 43%	α'_2	s^{-1}	656 ± 43%
β'_1	s^{-1}	30,600 ± 83%	β'_2	s^{-1}	57,300 ± 91%
γ''_2	s^{-1}	11,900 ± 30%	γ''_3	s^{-1}	12,000 ± 31%
δ''_2	s^{-1}	8,070 ± 27%	δ''_3	s^{-1}	8,330 ± 27%
γ'_2	s^{-1}	2,380 ± 35%	γ'_3	s^{-1}	2,530 ± 35%
δ'_2	s^{-1}	1,620 ± 31%	δ'_3	s^{-1}	1,830 ± 27%
γ'_1	s^{-1}	15,200 ± 84%	γ'_2	s^{-1}	29,300 ± 91%
δ'_1	s^{-1}	22 ± 48%	δ'_2	s^{-1}	33 ± 34%
k_-	s^{-1}	105 ± 5%	k_-	s^{-1}	83 ± 12%
k_+	M^{-1} s^{-1}	0.74×10^4 ± 32%	k_+	M^{-1} s^{-1}	1.20×10^4 ± 12%
k_{f-}	s^{-1}	299,000 ± 48%	k_{f-}	s^{-1}	207,000 ± 46%
k_{f+}	M^{-1} s^{-1}	3.83×10^9 ± 47%	k_{f+}	M^{-1} s^{-1}	5.36×10^9 ± 49%
$E''_2 = \beta''_2/\alpha''_2$		450 ± 17%	$E''_3 = \beta''_3/\alpha''_3$		450 ± 17%
$E'_2 = \beta'_2/\alpha'_2$		0.26 ± 26%	$E'_3 = \beta'_3/\alpha'_3$		0.27 ± 26%
$E'_1 = \beta'_1/\alpha'_1$		53 ± 73%	$E'_2 = \beta'_2/\alpha'_2$		97 ± 85%
$F''_2 = \delta''_2/\gamma''_2$		0.71± 16%	$F''_3 = \delta''_3/\gamma''_3$		0.72 ± 15%
$F'_2 = \delta'_2/\gamma'_2$		0.69 ± 10%	$F'_3 = \delta'_3/\gamma'_3$		0.76 ± 8%
$F'_1 = \delta'_1/\gamma'_1$		0.009 ± 89%	$F'_2 = \delta'_2/\gamma'_2$		0.013 ± 80%
$K_R = k_-/k_+$	mM	18 ± 37%	$K_R = k_-/k_+$	mM	7.1 ± 11%
$K_f = k_{f-}/k_{f+}$	mM	0.21 ± 82%	$K_f = k_{f-}/k_{f+}$	mM	0.14 ± 82%
E_{eff}		96 ± 13%	E_{eff}		102 ± 10%
EC_{50}	mM	1.4 ± 47%	EC_{50}	mM	1.4 ± 15%
n_H		1.84 ± 1%	n_H		2.5 ± 1%

The fits were constrained by the assumption that the binding sites are equivalent and independent. This constraint was implemented by the following equations: $k_{+1} = k_{+2} = k_{+3} = k_+$ and $k_{-1} = k_{-2} = k_{-3} = k_-$. In addition, one rate constant in each cycle was fixed by the constraint of microscopic reversibility (Colquhoun et al., 2004). The equilibrium constants *E*, *F*, and *K*, effective efficacy, E_{eff}, and the EC_{50} and Hill slope of the predicted P_{open} curve were calculated from the rate constants for each set and then averaged. Values are means ± coefficient of variation (i.e., SD of the mean expressed as a percentage of the mean).

Published December 29, 2014

sites plus desensitization) faithfully reproduces the time course of the experimental current (Fig. 9 D).

Fig. 9 E shows a comparison of the observed values of the current rise τ as a function of agonist concentration (black circles, one per patch, and short dash for the average) with the predictions of the best schemes (averages for the three fits). The schemes include variant Flip (Flip + O) and the Primed schemes with two or three binding sites, with or without empirical adjustment for macroscopic desensitization. The Flip + O scheme (3a in Fig. 4 and blue line in Fig. 9 E) predicted rise τ values that were consistently much faster than the ones we measured (this was also true for mechanisms 1 and 2 of Fig. 4; not depicted). The predictions of the variants of the Primed scheme were clearly better than Flip + O across all propylamine concentrations. Fig. 9 E shows Primed with two or three sites (green and red, respectively), with and without empirical correction for desensitization (dashed and solid, respectively). Fig. 9 F shows a comparison of the observed and predicted values for the deactivation τ calculated from the Flip + O and the Primed schemes (each point is calculated from the fit to an independent dataset). Predictions by all the variants of the Primed scheme were very good (but essentially equivalent for the two- and three-site variants), whereas those of the Flip + O scheme were much slower than the experimental values.

Prediction of burst length

One last set of experimental observations that should be accounted for by an adequate mechanism is the single-channel mean burst length. This is a useful additional comparison, because reliable burst length measurements can be obtained from recordings that contain too few events to be incorporated into the global mechanism fits, such as patches at 0.3 mM propylamine (trace in Fig. 10 B), where mean burst length is 140 ± 30 ms (213 bursts from three patches).

The Primed mechanism (Scheme 4, three sites) predicts that mean burst length should monotonically increase with agonist concentration (dashed line in Fig. 10 A). At low concentrations, the Scheme 4 predictions are very close to our observations (data are shown as closed circles in Fig. 10 A). Fig. 10 C depicts a simulation from Scheme 4 of single-channel currents at 0.3 mM propylamine,

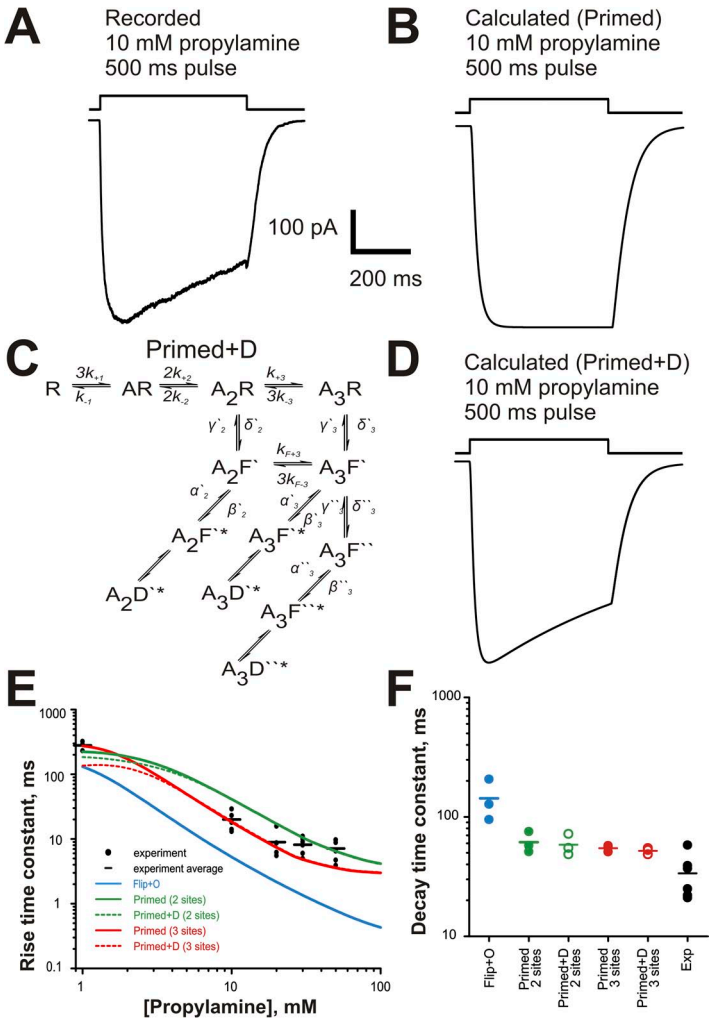

Figure 9. Primed activation schemes fitted to single-channel data predict the time course of macroscopic agonist responses. (A) ELIC inward current recorded in response to a 500-ms step of 10 mM propylamine applied to an outside-out patch (the square pulse above is the open-tip solution exchange measured at the end of the experiment). (B) Average macroscopic current calculated from the rate constants of the fit of the Primed mechanism (with three binding sites; Scheme 4) to the three sets of single-channel data in response to a 10-mM propylamine concentration jump (time constant of the solution exchange, 200 µs; top trace). (C) Scheme 4 + D shows the Primed mechanism modified by the empirical addition of desensitized states (D*) connected to the open states. (D) Average macroscopic current calculated from Scheme 4 + D, where the rate constants for entry and exit into desensitized states are empirically estimated from macroscopic data (see Results). (E) Experimental rise times for currents evoked by different agonist concentrations (black) compared with the predictions of the best schemes fitted to single-channel data. Closed circles are the experimental values, with the mean shown as a dash, and the colored curves are the average activation time constants calculated from the scheme fits to the single-channel data. The predictions of the Flip + O mechanism (Scheme 3a; blue) are consistently faster than the observed values, which are well predicted through the agonist concentration range by the Primed and Primed + D schemes (red for three sites and green for two sites, dashed if incorporating desensitization). (F) Dot plots showing the 20–80% decay time constant values measured in experimental responses to 10-mM concentration jumps (black) and in responses calculated from the mechanism fits (color coding as in E; dash shows the mean values; open symbols for the schemes incorporating desensitization).

Published December 29, 2014

and shows a mixture of short and long bursts similar to that observed in the experimental recording above (Fig. 10 B). However, at higher propylamine concentrations, the experimental mean burst length was much shorter than that predicted by the Primed mechanism. For example, the predicted burst length at 5 mM propylamine would be ~2.5 s, but the measured average burst length was 0.9 ± 0.3 s (t_{crit} = 10 ms; 56 bursts from three patches). The Primed scheme adjusted by the addition of macroscopic desensitization (Scheme 4 + D in Fig. 9 C) predicted very well the mean burst length at all propylamine concentrations (Fig. 10 A, solid line). This suggests that at higher concentrations, bursts can end not only by deactivation (e.g., agonist unbinding) but also by other ways that are not included in Scheme 4, for instance by desensitization, as clusters do. An interesting observation is that the average experimental burst length at 5 mM (~1 s) approaches the length of clusters at the higher concentrations, where clusters could be defined (e.g., at 10 mM, 2.2 ± 0.8 s, t_{crit} = 100 ms, 26 clusters from three patches; 50 mM, 1.0 ± 03 s, t_{crit} = 60 ms, 29 clusters from three patches).

This observation suggests that the number of bursts in each cluster must be very small, indeed that many clusters may contain a single burst. Measuring single-channel P_{open} relies on correctly identifying clusters versus bursts, and on obtaining clusters that contain a sufficient number of bursts. This could explain our difficulties in obtaining a P_{open} curve for ELIC. We explored the plausibility of this hypothesis by simulating single-channel activity with and without desensitization. The current traces in Fig. 10 (D and E) show 50 s of the activity of a single-channel molecule simulated for Schemes 4 and 5 in 1 mM propylamine (close to EC_{50}). When there is no desensitization (Fig. 10 D), the channel is open for ~50% of the time and produces bursts that are on average much longer than at 300 µM propylamine. When desensitization is added (Scheme 4 + D), the bursts clearly shorten and clusters start appearing (Fig. 10 E). However, most of the apparent clusters (defined by the longest shut intervals)

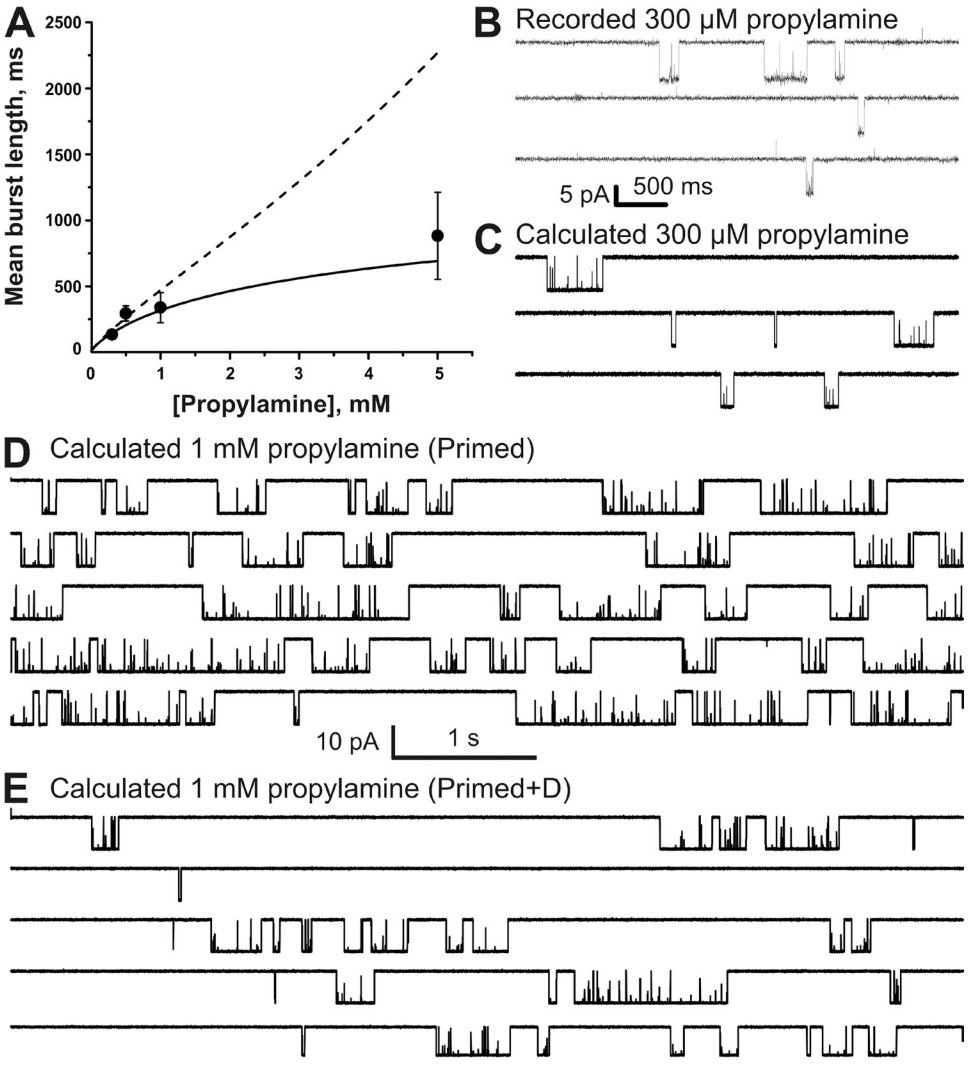

Figure 10. ELIC bursts can be ended by desensitization. (A) Observed values of ELIC mean burst length (closed circles; t_{crit} of 10 or 20 ms, depending on patch) are not well described at high propylamine concentrations by Scheme 4 (Primed; three binding sites), which predicts a linear increase in burst length with agonist concentration (dashed line). The same Primed scheme with the addition of desensitized states gives a better prediction of burst length (continuous curve), suggesting that desensitization can terminate bursts. (B) Traces are continuous sweeps of single-channel recordings at 0.3 mM propylamine (filtered at 3 kHz for display) from outside-out patches held at −60 mV. (C) Traces are continuous sweeps of single-channel activity calculated from Scheme 4 at 0.3 mM propylamine (3 kHz low-pass filter; one channel in the patch). Note the qualitative similarity between the experimental and the simulated trace at low concentration (compare the 0.3-mM point in A). (D and E) Traces are continuous sweeps of single-channel activity simulated at 1 mM propylamine from the two variants of the Primed mechanism, without desensitization and with desensitization (3 kHz low-pass filter; one channel in the patch).

Published December 29, 2014

do not contain a sufficient number of bursts to give a good estimate of the channel P_{open}. Many apparent clusters contain just a single burst and have nearly 100% P_{open}, and even clusters that do contain several bursts have P_{open} much higher than 50%. This qualitative example clearly shows that desensitization can terminate both bursts and clusters of bursts in ELIC, that it introduces ambiguity in choosing appropriate t_{crit} values for cluster separation, and that it consequently leads to strong overestimation of the channel P_{open}.

DISCUSSION

ELIC is a bacterial ligand-gated ion channel homologous to eukaryotic Cys-loop/nicotinic channels. It is found in the enterobacterium *E. chrysanthemi*, an important cause of soft rot in food and ornamental crops, but it is not clear whether ELIC itself is important for the pathogenicity of this prokaryote. ELIC is one of the four pLGIC family channels that have been imaged in their entirety and, as such, is an important source of structural information: crystal structures have been obtained for ELIC in an apo state (Hilf and Dutzler, 2008) or with ligands bound in the canonical agonist site, such as the agonists bromopropylamine and GABA (Zimmermann and Dutzler, 2011; Spurny et al., 2012), and the competitive antagonist acetylcholine (Pan et al., 2012). Structures have also been solved for ELIC bound to ligands that modulate the activity of channels in the nicotinic family, such as benzodiazepines and chloroform (Spurny et al., 2012, 2013), and divalent ions (Zimmermann et al., 2012). The consensus is that these structures all show the pore of ELIC in a nonconducting state (Hilf and Dutzler, 2008, 2009a; Song and Corry, 2010), but it remains unclear whether they represent resting or desensitized states (Gonzalez-Gutierrez et al., 2012).

Most of the published functional data from ELIC or from the other structural model channels GLIC and GluCl are macroscopic characterizations, and no kinetic model is available for any of these channels. ELIC appears to be the best candidate for a single-channel kinetic analysis because it is reported to have high single-channel conductance (84–96 pS) and to show only occasional subconductance transitions (Zimmermann and Dutzler, 2011), suggesting ideal signal-to-noise ratio for this technique. In contrast to that, the conductance of GLIC is low, only 8 pS in wild type (Bocquet et al., 2007), and to our knowledge there are no measurements of conductance for the form of GluCl whose crystal structure has been solved.

In addition to that, ELIC is the only one of these three channels that resembles vertebrate Cys-loop channels in being activated by the binding of a small molecule agonist to the canonical agonist-binding site in the extracellular domain (Zimmermann and Dutzler, 2011). Other structural model channels are different: GluCl is unusual, in that the form whose structure was solved (the α homomer) opens only if bound both to an orthosteric agonist, glutamate, and to ivermectin, an allosteric modulator that binds in the transmembrane domain (Hibbs and Gouaux, 2011). On the other hand, GLIC is not activated by a ligand but by low pH, and therefore by the protonation of amino acid side chains. The number and location of the residues that have to be protonated to elicit activation in GLIC are not known, but at least one is in the transmembrane domain, well away from the canonical agonist-binding site of the superfamily (Wang et al., 2012). This suggests that ELIC should offer the best model for a study aimed at understanding agonist efficacy in the context of channel structure.

The two most potent agonists for ELIC are reported to be cysteamine and propylamine (Zimmermann and Dutzler, 2011). We chose to use propylamine as an agonist in all of our experiments because cysteamine can be used only in the presence of millimolar concentrations of a reducing agent (to keep the sulphydryl group of the agonist in its reduced state). In addition to that, in our macroscopic records, the rebound current (see below) was more prominent when responses were elicited by cysteamine, arguing for a more potent block of the channel by this agonist.

Functional properties of ELIC

Our observations confirm and extend the description of the properties of ELIC from other laboratories, particularly with respect to slow activation and to the presence of slow but detectable desensitization (Gonzalez-Gutierrez and Grosman, 2010; Zimmermann and Dutzler, 2011; Laha et al., 2013). For a channel in the pLGIC family, ELIC activates remarkably slowly in response to agonists, with a limiting on-relaxation time constant of ∼10 ms to high concentrations of propylamine. ELIC is known to activate slowly in response to cysteamine, and the values reported for the limiting time constant of activation range from 20 to 85 ms in experimental conditions comparable to ours (e.g., rapid agonist application to outside-out patches; Zimmermann and Dutzler, 2011; Gonzalez-Gutierrez et al., 2012; Zimmermann et al., 2012; Laha et al., 2013). Activation is known to be slow also for the other prokaryotic model channel, GLIC, with limiting time constants between 10 and 150 ms (Gonzalez-Gutierrez et al., 2012; Velisetty and Chakrapani, 2012; Velisetty et al., 2012; Laha et al., 2013). Some of the variability may be caused by differences in the divalent ions in the recording medium (Spurny et al., 2012; Zimmermann et al., 2012).

We found that ELIC deactivation has a clearly sigmoidal time course. Detectably sigmoidal off-relaxations of agonist currents are reported for 5-HT_3A receptors and indeed GLIC (Corradi et al., 2009; Velisetty et al., 2012), suggesting that ELIC and these channels can reopen with good efficacy once the agonist pulse is over and when they have lost one or more of the full complement

Published December 29, 2014

of agonist molecules bound. In contrast to that, muscle nicotinic channels have a very low probability of opening when partially liganded (e.g., monoliganded) and do not have a sigmoidal deactivation (Maconochie and Steinbach, 1998). Interestingly, at saturating propylamine, the ELIC current rise time is monoexponential. This suggests that the paths followed by the channel through activation and deactivation by saturating propylamine are different.

The initial phase of the off-relaxation of ELIC agonist currents is notable for the presence of a rebound current; this is likely to be caused by the dissociation of agonist molecules from binding sites in the pore. The size of this current at 10 and 50 mM and the speed of its onset suggest a very low affinity, which we estimated to be 460 mM. The expected decrease in the amplitude of single-channel currents at the highest agonist concentrations used in the kinetic analysis is likely to be too small to be unambiguously detected in a channel like ELIC.

Our single-channel recordings confirm the report that ELIC channels open to a high main conductance (Zimmermann and Dutzler, 2011). Despite the favorable signal-to-noise ratio, ELIC proved to be a challenging subject for our kinetic analysis. Despite considerable effort, our recordings at agonist concentrations lower than the macroscopic EC_{50} (0.5 mM) had too few events to be usable in global model fits. At EC_{50}, one would expect to be able to identify desensitized clusters, groups of openings where a single-channel molecule opens at 50% P_{open} before entering a prolonged desensitized state. This proved impossible (cf. Fig. 3 A), and we failed to construct a concentration–P_{open} curve. Another unusual feature of ELIC single-channel activity was the presence of more than one open state at high agonist concentrations. ELIC shares both this property and a relatively weak dependence of pattern of openings upon agonist concentration with the homomeric α2 glycine receptor (Krashia et al., 2011).

The fitted models

We attempted to fit ELIC single-channel data with four types of models that are in general use to describe the behavior of Cys-loop channels. In their classical form, the simpler schemes, such as MWC, J&W, and Flip, failed to describe the main properties of the equilibrium single-channel data that they were fitted to. Because of the presence of more than one component in the ELIC open-time distributions at high propylamine, we modified these schemes by allowing fully liganded receptors to open to more than one state. Adding this extra open state is an arbitrary adjustment that sits uncomfortably with the physical picture of the process of channel activation implicit in each of these schemes. This addition improved the quality of the open-/shut-time description only for J&W and Flip: in the case of Flip + Open (Scheme 3a), the improvement was substantial, and the resulting fits were robust and consistent in their results across the three datasets, with a quality similar to that obtained by fitting the reduced Primed scheme (Scheme 4 and its variants). We then checked whether the results of the single-channel analysis could predict the on- and off-relaxations of macroscopic currents recorded in the same patch configuration from independent experiments. Only the Primed and the Flip + Open schemes gave predictions that approached the observed macroscopic rise and decay times. However, the Flip + Open scheme was worse than the Primed scheme, in that its predicted onset was consistently too fast and its predicted deactivation was too slow. The main difference between the Primed and the Flip + Open mechanisms is that the Primed contains an additional fully bound preopening intermediate (A_3F''). The connectivity of the Primed scheme may accommodate the features of ELIC better by allowing a greater difference between the activation and deactivation paths than the simpler Flip schemes.

Without launching into the realms of speculation, it is hard to picture what this ELIC requirement for Primed means in terms of the underlying protein conformational changes. This scheme was originally introduced to represent independent movement in the two binding sites of muscle nicotinic receptor and to allow the open states that stem from the priming of one or the other or both of the sites to have different stability (Mukhtasimova et al., 2009). Conversely, the Flip scheme resembles MWC, and depicts initial activation spreading as a concerted, all-or-none step that simultaneously increases binding affinity at all sites. Reality may fall somewhere between these extremes of total independence and infinite cooperativity, with some degree of site-to-site interaction, which may depend on the channel type and on whether the sites are adjacent. If the spread of activation across the sites is fast, the process may not be distinguishable from a concerted step, and Flip schemes may be sufficient to describe channel activation, because the recordings do not contain sufficient information to fit variants of the Primed mechanism.

We have seen that different channels are best fitted by different mechanisms (Primed to ELIC and to α1K276Eβ, Flip to glycine and muscle nicotinic wild-type channels). In particular, another relatively slow activating channel, the startle disease mutant of the glycine channel α1K276Eβ, also requires fitting with a Primed scheme, in this case an even more extreme form of the mechanism, with three fully bound intermediates (Lape et al., 2012). This mutant differs from ELIC in that it has a low maximum P_{open} but resembles ELIC in that it opens to multiple open states when fully liganded. In both cases, the Primed model interprets the multiple open states as openings that arise from different activation intermediates. The fit of the model shows that opening becomes more favorable as the channel progresses through the intermediate states.

ELIC activates maximally when agonist is bound to at least two and possibly three of the putative five binding

Published December 29, 2014

sites. We do not know whether a fourth and a fifth molecule bind, although structural data indicate that a related agonist, bromopropylamine, can occupy all five binding sites (Zimmermann and Dutzler, 2011). As for the glycine α1 homomeric channel, if they do bind, they do not detectably increase the stability of the open state (Beato et al., 2004; Burzomato et al., 2004). Three agonist molecules binding to five sites can bind in two different topologies, i.e., to consecutive or nonconsecutive sites. As elegantly shown by Rayes et al. (2009) for α7/5-HT_3 chimeras, it is possible that the nonconsecutive topology results in an open state that is more stable, and this could explain the presence of two open states at saturating agonist concentration. This hypothesis would be difficult to test by model fitting, as a scheme incorporating it would be grossly overparameterized.

Another difficult question is whether we can identify a structural reason for the slowness of ELIC. Most Cys-loop vertebrate channels reach maximum activation quickly, in less than a millisecond. It has been hypothesized that this is because of the presence in the extracellular domain of these channels of a water-filled cavity, which is absent in GLIC (Dellisanti et al., 2011). The ELIC extracellular domain is likely to be as tightly packed as that of GLIC, and ELIC resembles GLIC in lacking the two polar residues that are present in the most of the fast channels (except in the α-glycine subunits, which activate very fast but have hydrophobic residues in the homologous positions).

Keeping to safer ground, our results highlight several features of ELIC activity: the channel opens slowly, visiting at least two preopening intermediates before reaching a high maximum P_{open}. In its high maximum P_{open}, ELIC resembles other homomeric nicotinic-type channels, such as the different forms of glycine receptors (Beato et al., 2004; Burzomato et al., 2004; Krashia et al., 2011; Marabelli et al., 2013) and the 5-HT_3A receptor (Corradi et al., 2009). Full ELIC activation is reached when at least two and possibly three out of the five possible binding sites in the homomer are occupied by the agonist. Related homomeric channels such as α1 glycine receptors (Beato et al., 2004; Burzomato et al., 2004), α7 nicotinic (Rayes et al., 2009), and the 5-HT_3A receptor (Corradi et al., 2009) are thought to require the binding of three agonist molecules to activate fully.

Quantitative comparisons between the energy landscape for the activation of ELIC and that of other nicotinic-type channels have to be done with caution, because we can compare only the results of fits of similar models. This obliges us to use Flip-model variants (even though Flip + Open was inferior to Primed for ELIC), as fits of Primed schemes are not necessary to describe wild-type GlyRs. The main interesting feature that emerges is a clear resemblance between ELIC and α2 GlyR (Krashia et al., 2011), in that both channels have relatively poor flipping even when fully bound, compared with α1, α3, or α1β, with maximum flipping equilibrium constants of 0.4 and 1 (for ELIC and α2, respectively; cf. values of 8–11 for the α1 and α3 channels; Burzomato et al., 2004; Marabelli et al., 2013). Despite this disadvantaged flipping step (which resembles that seen with partial agonists on synaptic glycine receptors, e.g., taurine; Lape et al., 2008), both ELIC and α2 open with a high maximum P_{open} because of the very high equilibrium constant for the most efficacious opening step (500 and 350, respectively, cf. 38–80 for the α1 and α3 GlyR). This is largely because of a slow closing rate (120 and 370 s^{-1}, ELIC and α2 GlyR, respectively; cf. 700 and 2,400 s^{-1} for the α1 and α3 GlyRs). The opening rate for this step is fast for ELIC, with a value (62,000 s^{-1}) similar to those we estimated for other wild-type, nicotinic-type channels (between 28,000 and 150,000 s^{-1}).

The Primed mechanism and its predictions

Channels that are well behaved for kinetic analysis provide a concentration–P_{open} curve whose EC_{50} and slope are key in testing the adequacy of the fitted mechanisms, especially with respect to the number of agonist molecules needed for full activation and the values of the binding rate constants and their dependence on the state of ligation. Because this was not possible for ELIC, we tested further the Primed mechanism by examining its predictions of the results of independent experiments, where we measured the time course of macroscopic currents and the mean burst length at low concentrations. This allowed us not only to validate the model fitted and its estimates but also to gain insight into the cause of the difficulties that we encountered in our single-channel analysis. The main problem was that ELIC bursts are long and can be terminated by desensitization, a phenomenon described for other slow, high efficacy channels such as gain of function mutants of muscle nicotinics (Elenes et al., 2006). This leads to ambiguity in the classification of groups of openings as bursts or clusters (see Materials and methods). ELIC clusters are likely to contain few bursts, and this leads to problems in measuring P_{open} for nondesensitized states, as shown in Fig. 10. In addition to that, only the clusters that contain more than one burst will provide information on the interburst shut-time duration, which is the observable counterpart of the association rate constant. It was therefore important to check that the rate constant values obtained from single-channel fitting provided a good description of the on-relaxation of agonist currents at a range of concentrations. This is reassuring in terms of the accuracy of the results of our fits, and their robustness to ambiguities in classifying bursts and clusters.

How does the Primed scheme (Fig. 11 A) account for the most distinctive properties of ELIC, such as the concentration dependence of burst length and the time course of the on-and-off relaxation? A useful way of making sense of results of the fits is shown in Fig. 11 B,

Published December 29, 2014

where the numbers near the arrows are transition probabilities calculated from the primed rate constants at 0.1 and 10 mM propylamine (10-mM values are in bold; see Colquhoun and Lape, 2012). Note that rate constant values estimated using the Primed model with two binding sites were similar (Table 5), and would give rise to similar considerations.

The concentration dependence of ELIC burst length at equilibrium arises mainly from the concentration dependence of the agonist binding to the primed state A_2F' (in a manner similar to that we described for α2 glycine receptors; Krashia et al., 2011). Access to the main open state is via state A_3F', and this is reached by a different route at low versus high concentrations. At the lower concentrations, route $A_2R \rightarrow A_2F' \rightarrow A_3F'$ is favored over the alternative route $A_2R \rightarrow A_3R \rightarrow A_3F'$ (probabilities of 0.14 vs. 0.0017, respectively, at 100 µM propylamine). At 10 mM, both routes have similar probabilities, of 0.15 and 0.14, respectively. The receptor exits state A_3F' almost exclusively by unbinding an agonist molecule to reach state A_2F' (probability of 0.94). The probability of rebinding to this state is concentration dependent, and the increasing number of oscillations between states A_2F' and A_3F' accounts for the burst length increase with rising agonist concentrations.

Wyllie et al. (1998) have shown that the time constants of macroscopic off-relaxations to zero agonist are the same as those of the single-channel equilibrium burst length distribution at low concentration. We have an apparent discrepancy for ELIC, given that its overall deactivation time constant is 10–60 ms, and its mean burst length is 140 ms at the lowest agonist concentration that we could record. In this aspect, once again, ELIC closely resembles the α2 glycine receptor (Krashia et al., 2011). The Primed model results allow us to estimate that it would be necessary to record ELIC activity at around 10 µM propylamine to observe a mean burst length that matches the deactivation time constant.

At the end of the agonist concentration pulse, deactivation occurs almost exclusively via the return route $A_3F' \rightarrow A_2F' \rightarrow A_2R$, which has a probability of 0.32, 200-fold higher than the probability of the alternative route through the state A_3R. Because of that, although there can be no rebinding at zero agonist concentration, the receptor can open again. This is because the channel leaves state A_3F' through state A_2F', which can reopen to $A_2F'^*$ with a probability of 0.66 (at 0 mM). Because of the high efficacy (E_2' = 97) of this opening and the prolonged oscillations between states A_2F' and $A_2F'^*$, there can be significant opening at these partially bound states. The temporal accumulation of receptors in states A_2F' and $A_2F'^*$ on the deactivation path accounts for the sigmoidal shape of the ELIC macroscopic response decay.

Conclusions

We have shown that it is possible to describe ELIC macroscopic and single-channel activity with mechanistic schemes that are similar to those that are well established for other channels in the superfamily. ELIC opens in response to the binding of at least two and possibly three

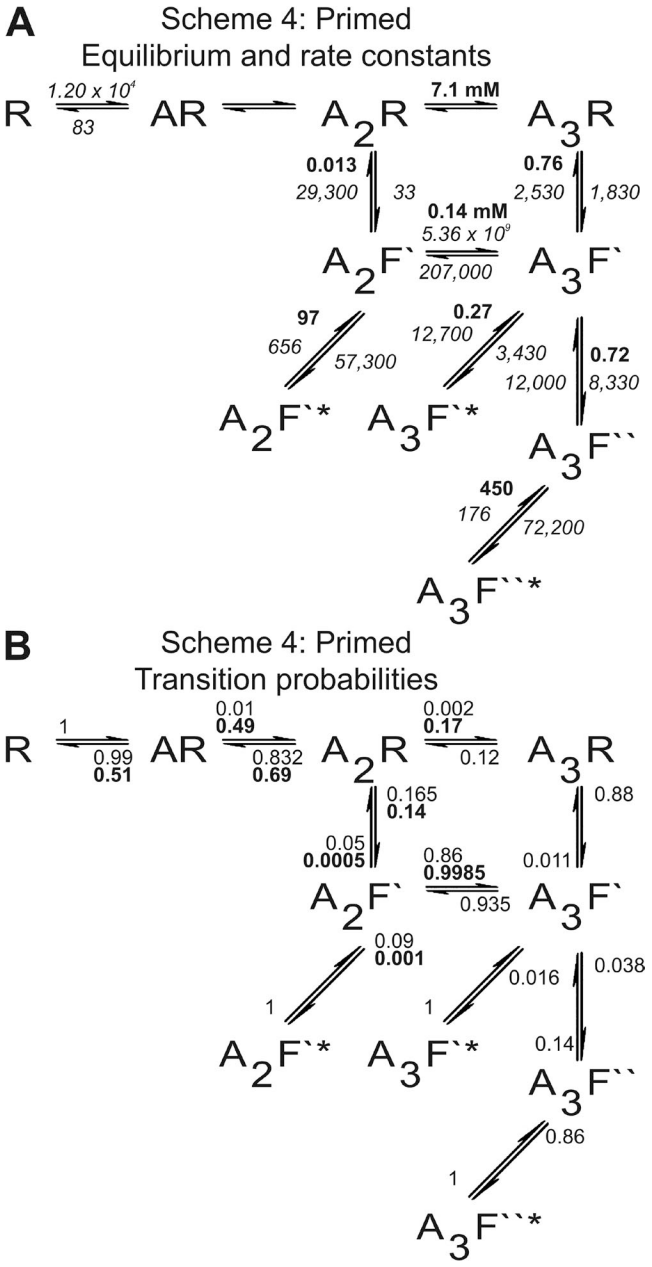

Figure 11. Summary of the Primed mechanism fitting results. (A) Rate constant values (units are s^{-1} or $M^{-1}\ s^{-1}$, if concentration dependent) are in italics, and equilibrium constants are in bold. Values of rate constants are means of three estimates, and values of equilibrium constants are ratios of mean values (see also Table 5). The rate constants in the cycle in this mechanism obeyed microscopic reversibility in each separate fit, but their averaging may affect this. (B) The transition arrows are marked with the transition probabilities between states. The probability values are shown for two concentrations: 0.1 and 10 mM (where the probability at 10 mM is in bold, when different from that at 0.1 mM). The transition probabilities are calculated using the mean rate constants in A. The sum of probabilities of transitions leading out of each state is 1.

propylamine molecules with high maximum P_{open}. Activation is relatively slow, mainly because the channel is slow in undergoing the initial preopening conformational changes. The fully bound channel can open to two open states.

ELIC presents some useful features for experimental kinetics (high single-channel conductance, activation slower than the technical limit of agonist solution exchange), but these are balanced by technical disadvantages. One clear difficulty arises from the long duration of activation bursts with respect to the duration of desensitized clusters. Consequently, each cluster contains at best a few bursts and interburst intervals, and that limits the information available to single-channel analysis on the binding steps in the reaction. This made it especially important for us to validate the single-channel model estimates against a wide range of data, including macroscopic current relaxations. This shows that establishing a detailed activation mechanism can be challenging when the channel properties are outside a fairly narrow "ideal" window, particularly for the values of the rate constants within the fitted scheme versus the desensitization rates. The glycine channel is almost ideal in this respect: ELIC is less than ideal. The best way forward may be to intervene by appropriate mutational engineering to shorten the burst length and make ELIC a more useful model channel for work on the structure–function relation in nicotinic-type channels.

We are grateful to Iwan Zimmermann and Raimund Dutzler (University of Zürich) for sharing ELIC constructs.

This work was funded by the Biotechnology and Biological Sciences Research Council (grant BB/J005312/1 to L. Sivilotti), and A. Marabelli received personal support by a University College London Impact studentship.

The authors declare no competing financial interests.

Author contributions: A. Marabelli and R. Lape collected the data. All authors contributed to the conception and design of the experiments, analysis, and interpretation of data, and to writing the article. All authors approved the final version of the manuscript for publication.

Merritt C. Maduke served as editor.

Submitted: 22 May 2014
Accepted: 17 November 2014

REFERENCES

Auerbach, A. 2012. Thinking in cycles: MWC is a good model for acetylcholine receptor-channels. *J. Physiol.* 590:93–98.

Beato, M., P.J. Groot-Kormelink, D. Colquhoun, and L.G. Sivilotti. 2004. The activation mechanism of α1 homomeric glycine receptors. *J. Neurosci.* 24:895–906. http://dx.doi.org/10.1523/JNEUROSCI.4420-03.2004

Bocquet, N., L. Prado de Carvalho, J. Cartaud, J. Neyton, C. Le Poupon, A. Taly, T. Grutter, J.-P. Changeux, and P.J. Corringer. 2007. A prokaryotic proton-gated ion channel from the nicotinic acetylcholine receptor family. *Nature.* 445:116–119. http://dx.doi.org/10.1038/nature05371

Bocquet, N., H. Nury, M. Baaden, C. Le Poupon, J.P. Changeux, M. Delarue, and P.J. Corringer. 2009. X-ray structure of a pentameric ligand-gated ion channel in an apparently open conformation. *Nature.* 457:111–114. http://dx.doi.org/10.1038/nature07462

Burzomato, V., M. Beato, P.J. Groot-Kormelink, D. Colquhoun, and L.G. Sivilotti. 2004. Single-channel behavior of heteromeric α1β glycine receptors: An attempt to detect a conformational change before the channel opens. *J. Neurosci.* 24:10924–10940. http://dx.doi.org/10.1523/JNEUROSCI.3424-04.2004

Colquhoun, D., and A.G. Hawkes. 1990. Stochastic properties of ion channel openings and bursts in a membrane patch that contains two channels: Evidence concerning the number of channels present when a record containing only single openings is observed. *Proc. R. Soc. Lond. B Biol. Sci.* 240:453–477. http://dx.doi.org/10.1098/rspb.1990.0048

Colquhoun, D., and R. Lape. 2012. Perspectives on: Conformational coupling in ion channels: Allosteric coupling in ligand-gated ion channels. *J. Gen. Physiol.* 140:599–612. http://dx.doi.org/10.1085/jgp.201210844

Colquhoun, D., A.G. Hawkes, and K. Srodzinski. 1996. Joint distributions of apparent open and shut times of single-ion channels and maximum likelihood fitting of mechanisms. *Philos. Trans. A Math. Phys. Eng. Sci.* 354:2555–2590. http://dx.doi.org/10.1098/rsta.1996.0115

Colquhoun, D., C.J. Hatton, and A.G. Hawkes. 2003. The quality of maximum likelihood estimates of ion channel rate constants. *J. Physiol.* 547:699–728. http://dx.doi.org/10.1113/jphysiol.2002.034165

Colquhoun, D., K.A. Dowsland, M. Beato, and A.J. Plested. 2004. How to impose microscopic reversibility in complex reaction mechanisms. *Biophys. J.* 86:3510–3518. http://dx.doi.org/10.1529/biophysj.103.038679

Corradi, J., F. Gumilar, and C. Bouzat. 2009. Single-channel kinetic analysis for activation and desensitization of homomeric 5-HT_3A receptors. *Biophys. J.* 97:1335–1345. http://dx.doi.org/10.1016/j.bpj.2009.06.018

Dellisanti, C.D., S.M. Hanson, L. Chen, and C. Czajkowski. 2011. Packing of the extracellular domain hydrophobic core has evolved to facilitate pentameric ligand-gated ion channel function. *J. Biol. Chem.* 286:3658–3670. http://dx.doi.org/10.1074/jbc.M110.156851

Elenes, S., Y. Ni, G.D. Cymes, and C. Grosman. 2006. Desensitization contributes to the synaptic response of gain-of-function mutants of the muscle nicotinic receptor. *J. Gen. Physiol.* 128:615–627. http://dx.doi.org/10.1085/jgp.200609570

Gonzalez-Gutierrez, G., and C. Grosman. 2010. Bridging the gap between structural models of nicotinic receptor superfamily ion channels and their corresponding functional states. *J. Mol. Biol.* 403:693–705. http://dx.doi.org/10.1016/j.jmb.2010.09.026

Gonzalez-Gutierrez, G., T. Lukk, V. Agarwal, D. Papke, S.K. Nair, and C. Grosman. 2012. Mutations that stabilize the open state of the *Erwinia chrisanthemi* ligand-gated ion channel fail to change the conformation of the pore domain in crystals. *Proc. Natl. Acad. Sci. USA.* 109:6331–6336. http://dx.doi.org/10.1073/pnas.1119268109

Groot-Kormelink, P.J., M. Beato, C. Finotti, R.J. Harvey, and L.G. Sivilotti. 2002. Achieving optimal expression for single channel recording: a plasmid ratio approach to the expression of α1 glycine receptors in HEK293 cells. *J. Neurosci. Methods.* 113:207–214. http://dx.doi.org/10.1016/S0165-0270(01)00500-3

Grosman, C., M. Zhou, and A. Auerbach. 2000. Mapping the conformational wave of acetylcholine receptor channel gating. *Nature.* 403:773–776. http://dx.doi.org/10.1038/35001586

Hawkes, A.G., A. Jalali, and D. Colquhoun. 1990. The distributions of the apparent open times and shut times in a single channel record when brief events cannot be detected. *Philos. Trans. A Math. Phys. Eng. Sci.* 332:511–538. http://dx.doi.org/10.1098/rsta.1990.0129

Hawkes, A.G., A. Jalali, and D. Colquhoun. 1992. Asymptotic distributions of apparent open times and shut times in a single channel record allowing for the omission of brief events. *Philos. Trans. R. Soc. Lond. B Biol. Sci.* 337:383–404. http://dx.doi.org/10.1098/rstb.1992.0116

Hibbs, R.E., and E. Gouaux. 2011. Principles of activation and permeation in an anion-selective Cys-loop receptor. *Nature.* 474:54–60. http://dx.doi.org/10.1038/nature10139

Hilf, R.J., and R. Dutzler. 2008. X-ray structure of a prokaryotic pentameric ligand-gated ion channel. *Nature.* 452:375–379. http://dx.doi.org/10.1038/nature06717

Hilf, R.J., and R. Dutzler. 2009a. A prokaryotic perspective on pentameric ligand-gated ion channel structure. *Curr. Opin. Struct. Biol.* 19:418–424. http://dx.doi.org/10.1016/j.sbi.2009.07.006

Hilf, R.J., and R. Dutzler. 2009b. Structure of a potentially open state of a proton-activated pentameric ligand-gated ion channel. *Nature.* 457:115–118. http://dx.doi.org/10.1038/nature07461

Jadey, S., and A. Auerbach. 2012. An integrated catch-and-hold mechanism activates nicotinic acetylcholine receptors. *J. Gen. Physiol.* 140:17–28. http://dx.doi.org/10.1085/jgp.201210801

Jones, M.V., and G.L. Westbrook. 1995. Desensitized states prolong $GABA_A$ channel responses to brief agonist pulses. *Neuron.* 15:181–191. http://dx.doi.org/10.1016/0896-6273(95)90075-6

Krashia, P., R. Lape, F. Lodesani, D. Colquhoun, and L.G. Sivilotti. 2011. The long activations of α2 glycine channels can be described by a mechanism with reaction intermediates ("flip"). *J. Gen. Physiol.* 137:197–216. http://dx.doi.org/10.1085/jgp.201010521

Krishtal, O.A., and V.I. Pidoplichko. 1980. A receptor for protons in the nerve cell membrane. *Neuroscience.* 5:2325–2327. http://dx.doi.org/10.1016/0306-4522(80)90149-9

Laha, K.T., B. Ghosh, and C. Czajkowski. 2013. Macroscopic kinetics of pentameric ligand gated ion channels: Comparisons between two prokaryotic channels and one eukaryotic channel. *PLoS ONE.* 8:e80322. http://dx.doi.org/10.1371/journal.pone.0080322

Lape, R., D. Colquhoun, and L.G. Sivilotti. 2008. On the nature of partial agonism in the nicotinic receptor superfamily. *Nature.* 454:722–727.

Lape, R., P. Krashia, D. Colquhoun, and L.G. Sivilotti. 2009. Agonist and blocking actions of choline and tetramethylammonium on human muscle acetylcholine receptors. *J. Physiol.* 587:5045–5072. http://dx.doi.org/10.1113/jphysiol.2009.176305

Lape, R., A.J.R. Plested, M. Moroni, D. Colquhoun, and L.G. Sivilotti. 2012. The α1K276E startle disease mutation reveals multiple intermediate states in the gating of glycine receptors. *J. Neurosci.* 32:1336–1352. http://dx.doi.org/10.1523/JNEUROSCI.4346-11.2012

Legendre, P., D.W. Ali, and P. Drapeau. 2000. Recovery from open channel block by acetylcholine during neuromuscular transmission in zebrafish. *J. Neurosci.* 20:140–148.

Maconochie, D.J., and J.H. Steinbach. 1995. Block by acetylcholine of mouse muscle nicotinic receptors, stably expressed in fibroblasts. *J. Gen. Physiol.* 106:113–147. http://dx.doi.org/10.1085/jgp.106.1.113

Maconochie, D.J., and J.H. Steinbach. 1998. The channel opening rate of adult- and fetal-type mouse muscle nicotinic receptors activated by acetylcholine. *J. Physiol.* 506:53–72. http://dx.doi.org/10.1111/j.1469-7793.1998.053bx.x

Marabelli, A., M. Moroni, R. Lape, and L.G. Sivilotti. 2013. The kinetic properties of the α3 rat glycine receptor make it suitable for mediating fast synaptic inhibition. *J. Physiol.* 591:3289–3308.

Monod, J., J. Wyman, and J.-P. Changeux. 1965. On the nature of allosteric transitions: A plausible model. *J. Mol. Biol.* 12:88–118. http://dx.doi.org/10.1016/S0022-2836(65)80285-6

Mukhtasimova, N., W.Y. Lee, H.L. Wang, and S.M. Sine. 2009. Detection and trapping of intermediate states priming nicotinic receptor channel opening. *Nature.* 459:451–454. http://dx.doi.org/10.1038/nature07923

Pan, J., Q. Chen, D. Willenbring, K. Yoshida, T. Tillman, O.B. Kashlan, A. Cohen, X.P. Kong, Y. Xu, and P. Tang. 2012. Structure of the pentameric ligand-gated ion channel ELIC cocrystallized with its competitive antagonist acetylcholine. *Nat. Commun.* 3:714. http://dx.doi.org/10.1038/ncomms1703

Purohit, P., A. Mitra, and A. Auerbach. 2007. A stepwise mechanism for acetylcholine receptor channel gating. *Nature.* 446:930–933. http://dx.doi.org/10.1038/nature05721

Rayes, D., M.J. De Rosa, S.M. Sine, and C. Bouzat. 2009. Number and locations of agonist binding sites required to activate homomeric Cys-loop receptors. *J. Neurosci.* 29:6022–6032. http://dx.doi.org/10.1523/JNEUROSCI.0627-09.2009

Sakmann, B., J. Patlak, and E. Neher. 1980. Single acetylcholine-activated channels show burst-kinetics in presence of desensitizing concentrations of agonist. *Nature.* 286:71–73. http://dx.doi.org/10.1038/286071a0

Sauguet, L., A. Shahsavar, F. Poitevin, C. Huon, A. Menny, À. Nemecz, A. Haouz, J.P. Changeux, P.J. Corringer, and M. Delarue. 2014. Crystal structures of a pentameric ligand-gated ion channel provide a mechanism for activation. *Proc. Natl. Acad. Sci. USA.* 111:966–971. http://dx.doi.org/10.1073/pnas.1314997111

Sivilotti, L.G. 2010. What single-channel analysis tells us of the activation mechanism of ligand-gated channels: the case of the glycine receptor. *J. Physiol.* 588:45–58. http://dx.doi.org/10.1113/jphysiol.2009.178525

Song, C., and B. Corry. 2010. Ion conduction in ligand-gated ion channels: Brownian dynamics studies of four recent crystal structures. *Biophys. J.* 98:404–411. http://dx.doi.org/10.1016/j.bpj.2009.10.032

Spurny, R., J. Ramerstorfer, K. Price, M. Brams, M. Ernst, H. Nury, M. Verheij, P. Legrand, D. Bertrand, S. Bertrand, et al. 2012. Pentameric ligand-gated ion channel ELIC is activated by GABA and modulated by benzodiazepines. *Proc. Natl. Acad. Sci. USA.* 109:E3028–E3034. http://dx.doi.org/10.1073/pnas.1208208109

Spurny, R., B. Billen, R.J. Howard, M. Brams, S. Debaveye, K.L. Price, D.A. Weston, S.V. Strelkov, J. Tytgat, S. Bertrand, et al. 2013. Multisite binding of a general anesthetic to the prokaryotic pentameric *Erwinia chrysanthemi* ligand-gated ion channel (ELIC). *J. Biol. Chem.* 288:8355–8364. http://dx.doi.org/10.1074/jbc.M112.424507

Velisetty, P., and S. Chakrapani. 2012. Desensitization mechanism in prokaryotic ligand-gated ion channel. *J. Biol. Chem.* 287:18467–18477. http://dx.doi.org/10.1074/jbc.M112.348045

Velisetty, P., S.V. Chalamalasetti, and S. Chakrapani. 2012. Conformational transitions underlying pore opening and desensitization in membrane-embedded *Gloeobacter violaceus* ligand-gated ion channel (GLIC). *J. Biol. Chem.* 287:36864–36872. http://dx.doi.org/10.1074/jbc.M112.401067

Wang, H.L., X. Cheng, and S.M. Sine. 2012. Intramembrane proton binding site linked to activation of bacterial pentameric ion channel. *J. Biol. Chem.* 287:6482–6489. http://dx.doi.org/10.1074/jbc.M111.305839

Wyllie, D.J., P. Béhé, and D. Colquhoun. 1998. Single-channel activations and concentration jumps: comparison of recombinant NR1a/NR2A and NR1a/NR2D NMDA receptors. *J. Physiol.* 510:1–18. http://dx.doi.org/10.1111/j.1469-7793.1998.001bz.x

Zimmermann, I., and R. Dutzler. 2011. Ligand activation of the prokaryotic pentameric ligand-gated ion channel ELIC. *PLoS Biol.* 9:e1001101. http://dx.doi.org/10.1371/journal.pbio.1001101

Zimmermann, I., A. Marabelli, C. Bertozzi, L.G. Sivilotti, and R. Dutzler. 2012. Inhibition of the prokaryotic pentameric ligand-gated ion channel ELIC by divalent cations. *PLoS Biol.* 10:e1001429. http://dx.doi.org/10.1371/journal.pbio.1001429